

The Charged Higgs from the Bottom-Up: Probing Flavor at the LHC

Nishita Desai,^a Alberto Mariotti,^b Mustafa Tabet,^c Robert Ziegler,^d

^a*Tata Institute of Fundamental Research, Homi Bhabha Road, Mumbai 400005, India*

^b*Theoretische Natuurkunde and IIHE/ELEM, Vrije Universiteit Brussel,
& The International Solvay Institutes, Pleinlaan 2, B-1050 Brussels, Belgium*

^b*Fakultät für Physik, TU Dortmund, D-44221 Dortmund, Germany*

^d*Institut für Theoretische Teilchenphysik, Karlsruhe Institute of Technology (KIT),
76128 Karlsruhe, Germany*

E-mail: desai@theory.tifr.res.in, alberto.mariotti@vub.be,
mustafa.tabet@tu-dortmund.de, robert.ziegler@kit.edu

ABSTRACT: We systematically study model-independent constraints on the three generic charged Higgs couplings to b -quarks and up-type quarks. While existing LHC searches have focussed on the tb coupling, we emphasize that the LHC plays a crucial role in probing also ub and cb couplings, since constraints from flavor physics are weak. In particular we propose various new searches that can significantly extend the present reach on the parameter space by: i) looking for light charged Higgses that decay into ub -quarks, ii) probing charged Higgs couplings to light and top quarks using multi- b -jet signatures, iii) looking for single b -quarks in low-mass dijet searches, iv) searching for charge asymmetries induced by charged Higgs production via ub couplings.

Contents

1	Introduction	2
2	Flavor Constraints	4
2.1	$D-\bar{D}$ mixing	4
2.2	Rare top decays	4
3	Collider Constraints on Production and Decay Topologies	5
3.1	Constraints on $tb \rightarrow H^\pm \rightarrow tb$	5
3.2	Constraints on $tb \rightarrow H^\pm \rightarrow qb$	6
3.3	Constraints on $qb \rightarrow H^\pm \rightarrow qb$	7
3.4	Constraints on $qb \rightarrow H^\pm \rightarrow tb$	10
3.5	Charge asymmetry	14
4	Constraints on Charged Higgs Couplings	16
5	Summary and Conclusions	21
A	Validation of PYTHIA code used for $qb \rightarrow H^\pm \rightarrow qb$ analysis	22
B	Validation of PYTHIA code used for $qb \rightarrow H^\pm \rightarrow tb$ analysis	22
B.1	Validation with arXiv:1209.4397 (CMS)	22
B.2	Validation with arXiv:1512.03704 (ATLAS)	23
C	BDT analysis of $qb \rightarrow H^\pm \rightarrow tb$ signature	24

1 Introduction

Extended Higgs sectors are ubiquitous in theories beyond the Standard Model (SM), and might play an important role to solve long-standing problems in particle physics, such as the stability of the electroweak scale [1], the nature of Dark Matter (DM) [2], the absence of CP violation in strong interactions [3, 4], or the origin of the matter/anti-matter asymmetry [5]. Accordingly, the experimental collaborations have been actively searching for additional Higgs bosons at colliders, resulting in stringent constraints on common benchmark models, such as the so-called Type I and II two Higgs doublet models (2HDM), which by construction avoid the appearance of large flavor-changing neutral currents [6]. However, it is fairly easy to evade the standard collider bounds on additional neutral and charged Higgs bosons by allowing for sizable flavor-changing interactions [7], which at the same time are consistent with constraints from precision flavor physics. Such interactions are present in the very general class of Type-III 2HDMs, and are controlled by a plethora of free parameters that gives rise to an extremely rich phenomenology [8, 9]. It is essential to be aware of these possibilities when designing experimental search strategies aiming to cover the blind spots of traditional searches.

Specific pattern of flavor violation have been employed in numerous scenarios motivated by outstanding theoretical problems and/or experimental anomalies. Flavor-changing couplings of light additional Higgs fields have been considered for example in QCD axion models (accounting for both Strong CP and DM) [10, 11], scenarios of Electroweak Baryogenesis [12–15], and models addressing fermion mass hierarchies [16–21] or the origin of CP violation in the Yukawa sector [22, 23]. Similar setups have been used to explain the anomalous magnetic moment of the muon [24–26] or the various anomalies observed in semi-leptonic B -meson decays [27–33]. Phenomenological aspects of these scenarios have been studied in e.g. Refs. [34–53]. Given the broad spectrum of theoretically motivated scenarios and phenomenological implications, it is appropriate to use a model-independent approach focussing on a specific sector of flavor-violating Higgs couplings, in the same spirit as e.g. Ref. [7].

In the present work we analyze the present experimental constraints and future prospects on generic couplings of a charged Higgs boson to b -quarks, described by the simplified Lagrangian

$$\mathcal{L} = H^+ (g_{tb}\bar{t}_R b_L + g_{cb}\bar{c}_R b_L + g_{ub}\bar{u}_R b_L) + \text{h.c.} - m_{H^\pm}^2 H^+ H^- . \quad (1.1)$$

We neglect H^+ couplings to right-handed b -quarks because they are connected to flavor-violating couplings of neutral Higgses to down-type quarks, which are strongly constrained by flavor physics¹. We also ignore charged Higgs couplings to leptons, which could play an important role in scenarios explaining the current anomalies in $R_{D^{(*)}}$ measured at the B -factories (see e.g. Ref. [52]). Here instead we focus on the case where such couplings are sufficiently small such that the charged Higgs decays dominantly into quarks. A particularly motivated UV scenario behind the Lagrangian in Eq. (1.1) is provided by the class of models

¹The couplings in Eq. (1.1) instead are connected to flavor-violating couplings of neutral Higgses to up-type quarks, which are only weakly constrained by flavor observables.

in Ref. [23], which induces the CKM phase by spontaneous CP violation at the electroweak scale. Interestingly, this implies both an upper bound on the charged Higgs mass of about 430 GeV and a lower bound on its couplings to b -quarks, $\max(|g_{tb}|, |g_{cb}|, |g_{ub}|) \geq 0.20$.

The couplings in Eq. (1.1) are only weakly constrained by flavor physics, as D - \bar{D} mixing only probes the combination $g_{ub}g_{cb}$ and top decays such as $t \rightarrow u\gamma, c\gamma$ give negligible constraints. Therefore bounds from direct searches at colliders are crucial in order to probe charged Higgs couplings to b -quarks. In the following we study these constraints using (and recasting) existing searches at the LHC. They can be classified according to the production and decay topology²:

- | | |
|--|--|
| 1) top associated production and top decay | $tb \rightarrow H^\pm \rightarrow tb,$ |
| 2) top associated production and light quark decay | $tb \rightarrow H^\pm \rightarrow qb,$ |
| 3) light quark production and decay | $qb \rightarrow H^\pm \rightarrow qb,$ |
| 4) light quark production and top decay | $qb \rightarrow H^\pm \rightarrow tb,$ |

where $q = u, c$, since it is typically difficult to distinguish up and charm quarks [54–56].

Out of these general topologies, at present only top production and decay has been studied by the experimental collaborations [57, 58], in addition to top production and cb decay when the decay to tb is kinematically forbidden [59]. Signal topologies with only light quarks have not been explicitly searched for, but can be constrained by recasting dijet constraints on Z' models [60–64] (see also Ref. [51]). In this work we systematically include all available channels to derive constraints on the generic couplings in Eq. (1.1). Moreover, we suggest to extend existing experimental searches in several ways: **1)** we propose to carry out a search for $tb \rightarrow H^\pm \rightarrow ub$ in a similar way to the existing search for $tb \rightarrow H^\pm \rightarrow cb$, **2)** we suggest to perform dedicated searches for charged Higgses coupling dominantly to light quarks, $qb \rightarrow H^\pm \rightarrow qb$, using single b -quark tagging, **3)** we study the potential to test the top decay channels $qb \rightarrow H^\pm \rightarrow tb$ using multi- b -jet signatures (as has been proposed also in Ref. [48]), and finally **4)** we study the possibility to distinguish c - and u -quarks in $qb \rightarrow H^\pm \rightarrow tb$ using charge asymmetries.

This work is structured as follows: In Section 2 we study the flavor constraints from D - \bar{D} mixing and top decays. In Section 3 we discuss the existing collider constraints for the four production and decay topologies above, and propose various new searches that could significantly increase sensitivity. In particular we study the potential to use lepton charge asymmetries in order to distinguish ub from cb production and reduce background. In Section 4 we express the constraints on the various signal topologies at colliders as model-independent bounds on the Lagrangian couplings in Eq. (1.1), also combining with the constraints from flavor physics. We summarize our results in Section 5. In Appendix A and B we provide validations of the PYTHIA code used in our analyses for $qb \rightarrow H^\pm \rightarrow qb$ and $qb \rightarrow H^\pm \rightarrow tb$, respectively, while Appendix C contains the details on multivariate analysis for the $qb \rightarrow H^\pm \rightarrow tb$ based on a boosted-decision-tree algorithm.

²We classify the topologies on the quark level, which is just a shorthand for the corresponding LHC process, e.g. $qb \rightarrow H^\pm \rightarrow qb$ stands for $pp \rightarrow (j)H^\pm(\rightarrow qb)$, where (j) denotes possible extra jets, while $tb \rightarrow H^\pm \rightarrow tb$ stands for $pp \rightarrow tbH^\pm(\rightarrow tb)$.

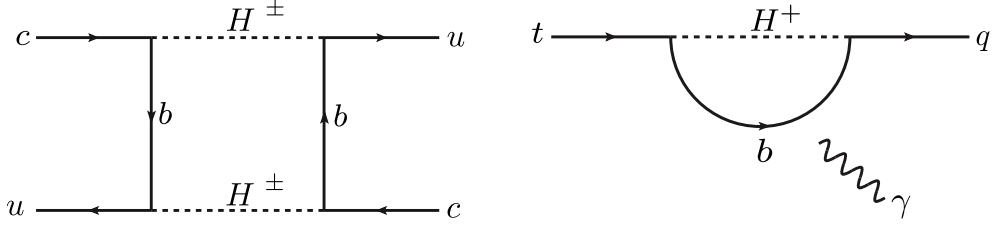


Figure 1. Box diagram contributing to $D-\bar{D}$ mixing (left), and photon penguin inducing rare top decays $t \rightarrow q\gamma$, $q = u, c$ (right), where the photon is attached to any charged particle.

2 Flavor Constraints

Box diagrams with charged Higgs exchange provide constraints on the combination $g_{ub}g_{cb}$ from $D-\bar{D}$ mixing, while radiative top decays $t \rightarrow c\gamma$ ($t \rightarrow u\gamma$) constrain the combination $g_{tb}g_{cb}$ ($g_{tb}g_{ub}$). Only the former provide relevant bounds, as we discuss in the following.

2.1 $D-\bar{D}$ mixing

The dominant contribution to $D-\bar{D}$ mixing comes from the charged Higgs box diagram in Fig. 1, which contributes to the effective $\Delta C = 2$ operator O'_1 . Assuming that new physics contributions to the absorptive part of the mixing amplitude Γ_{12}^{NP} in the neutral D -meson system are negligible, the relevant constraints arise from charged Higgs contributions to the dispersive part of the mixing amplitude M_{12}^{NP}

$$M_{12}^{\text{NP}} = \frac{1}{2M_D} \langle D | H^{\text{NP}, |\Delta C|=2} | \bar{D} \rangle = \frac{\eta g_{cb}^2 g_{ub}^{*2}}{128\pi^2 m_{H^\pm}^2} f \left(\frac{m_b^2}{m_{H^\pm}^2} \right) \text{GeV}^3, \quad (2.1)$$

where $\eta \approx 0.021$ includes the hadronic quantities and the QCD running and the loop function is $f(x) = (1 + 2x \log x - x^2) / (1 - x)^3$.

Since the SM contribution is dominated by long-distance contributions and no reliable estimates are available, we constrain the charged Higgs contribution to the mixing amplitude to lie below the experimental value at 95% CL, which is taken from the online update of the UTfit collaboration [65, 66]

$$|M_{12}|_{95\%} < 0.0079 \text{ps}^{-1} = 5.2 \times 10^{-15} \text{GeV}. \quad (2.2)$$

We show the allowed region in the parameter space in Fig. 2 for fixed charged Higgs masses, to which the constraints are roughly proportional.

2.2 Rare top decays

The charged Higgs contribution to the rare top decays $t \rightarrow c(u)\gamma$ in Fig. 1 gives a constraint on the combination $g_{tb}g_{c(u)b}$. The current experimental upper limits at 95% CL are [67]

$$\begin{aligned} \text{BR}_{\text{exp}}(t \rightarrow u\gamma) &= 6.1 \times 10^{-5}, \\ \text{BR}_{\text{exp}}(t \rightarrow c\gamma) &= 1.8 \times 10^{-4}. \end{aligned} \quad (2.3)$$

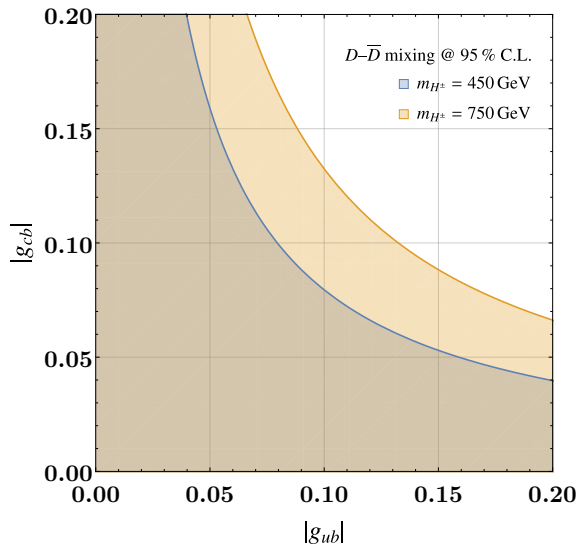


Figure 2. Region in the g_{ub} - g_{cb} plane allowed by D -meson mixing at 95% CL. The constraint on the product of both couplings scales linearly with the charged Higgs mass to very good approximation.

The charged Higgs contribution is given by

$$\text{BR}(t \rightarrow q\gamma) = \frac{m_t^5}{4\pi\Gamma_t} \left(\frac{5e}{1152\pi^2 m_{H^\pm}^2} \right)^2 |g_{tb}g_{qb}^*|^2, \quad (2.4)$$

giving $\text{BR}(t \rightarrow q\gamma) \sim 10^{-6}$ for a charged Higgs mass as light as 100 GeV and $\mathcal{O}(1)$ couplings. Therefore no relevant constraint are currently given by these rare top decays.

3 Collider Constraints on Production and Decay Topologies

In the following we discuss the collider constraints for all possible production and decay topologies, assuming 100% BR in the decay. We will mostly work in the four-flavor-scheme (4FS), except explicitly stated.

3.1 Constraints on $tb \rightarrow H^\pm \rightarrow tb$

Searches for charged Higgs bosons that couple mainly to the third generation have been performed both by ATLAS and CMS, looking for multijet events with one lepton and at least 2 b -jets. The best constraints arise from ATLAS searches at $\sqrt{s} = 13$ TeV employing the full Run 2 dataset of 139 fb^{-1} [57], while at present the CMS analysis is based only on 35.9 fb^{-1} [58]. We therefore use only the ATLAS results, which are presented as constraints on the product of the cross section of charged Higgs in association with top and bottom quarks $\sigma(pp \rightarrow \bar{t}bH^+)$, see Fig. 3, and the branching ratio of the charged Higgs decay $\text{BR}(H^+ \rightarrow t\bar{b})$. We re-interpret this analysis in terms of a constraint on the coupling g_{tb} in Eq. (1.1) using the LO cross-sections calculated with `MadGraph5_aMC@NLO` [68, 69] and an approximate K-factor of $K = 1.6$ [70]. The resulting NLO cross-section is used to obtain the 95% CL bounds on g_{tb} shown in Fig. 4.

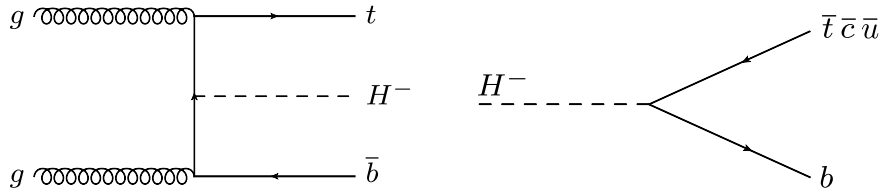


Figure 3. Charged Higgs production in association with top and bottom quarks (left) and charged Higgs decay into up-type and bottom quarks (right).

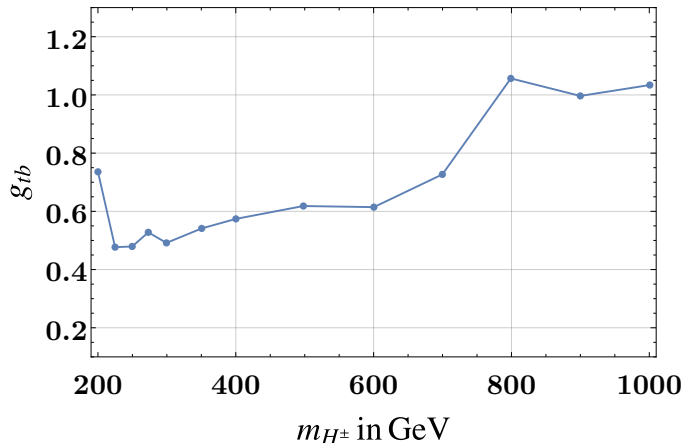


Figure 4. 95% CL Bounds on charged Higgs couplings g_{tb} from top production and decay derived from the ATLAS analysis in Ref. [57].

3.2 Constraints on $tb \rightarrow H^\pm \rightarrow qb$

If the charged Higgs decays mainly to light quarks, but is dominantly produced via its couplings to the top quark, then there has to be a strong hierarchy $g_{qb} \ll g_{tb}$ and the decay to top quarks must be kinematically closed, so that the charged Higgs is produced mainly via top decays. This topology has been searched for both at CMS [59] and ATLAS [71], giving upper limits on the branching ratio product $\text{BR}(t \rightarrow H^\pm b) \times \text{BR}(H^\pm \rightarrow cb)$ in the mass range 90–150 GeV (CMS) and 60–160 GeV (CMS). While the CMS search has used 19.7 fb^{-1} of data collected at $\sqrt{s} = 8 \text{ TeV}$, the ATLAS analysis is based on a data with $\sqrt{s} = 13 \text{ TeV}$ and an integrated luminosity of 139 fb^{-1} . Thanks to the larger dataset and refined analysis techniques, the ATLAS search has improved the sensitivity with respect to the CMS analysis by about a factor of five, and also explored a larger m_{H^\pm} range. For this reason we only use the ATLAS results in Ref. [71].

This analysis focusses on data enriched in top-quark pair production, where one top quark decays into a leptonically decaying W -boson and a bottom quark, and the other top quark decays into a charged Higgs boson and a bottom quark. This topology leads to a lepton-plus-jets final state, characterised by an isolated electron or muon and at least four jets, with a high multiplicity of b -jets, and missing energy. A neural network classifier is employed to distinguish between signal and background using kinematic differences. There is an irreducible SM background from $t\bar{t}$ production with a W -boson decaying to cb , which

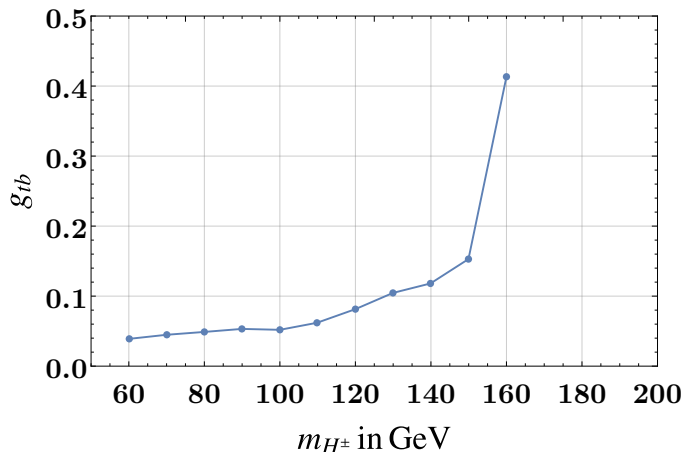


Figure 5. 95% CL constraints on charged Higgs couplings g_{tb} from top production and decay to cb , using the ATLAS analysis in Ref. [71]. These constraints are valid as long as g_{cb} (and g_{ub}) are sufficiently small such that H^\pm production is dominated by top decays.

is however suppressed by the corresponding small CKM element.

The resulting ATLAS limits on the branching ratios $\text{BR}(t \rightarrow H^\pm b) \times \text{BR}(H^\pm \rightarrow cb)$ can be interpreted as upper limits on the top coupling g_{tb} , assuming $\text{BR}(t \rightarrow H^\pm b) + \text{BR}(t \rightarrow W^\pm b) = \text{BR}(H^\pm \rightarrow cb) = 1$. These bounds are valid as long as the couplings g_{ub}, g_{cb} are small enough such that the top decays dominate the production. The resulting 95% CL limits on g_{tb} are shown in Fig. 5.

While the ATLAS analysis in Ref. [71] has focussed on $H^\pm \rightarrow cb$ decays, it could be worthwhile to perform a similar analysis on the same data set looking for $H^\pm \rightarrow ub$ decays. We presume such an analysis to be very similar, possibly even using the same signal categories, since the only difference is a light jet instead of a charm-jet. The ATLAS analysis was using a neural network exploiting the b -tagging score of this charm-jet, which helps to distinguish the signal from the main backgrounds, $t\bar{t}$ + light jets and $t\bar{t}$ + b -jets. Replacing the charm-jet by a light jet will presumably worsen the separation of the signal from the first background, but improve the separation from the latter background³. Thus one might expect that overall these effects would balance and the proposed analysis might lead to constraints on $\text{BR}(t \rightarrow H^\pm b) \times \text{BR}(H^\pm \rightarrow ub)$ that are as stringent than those on $\text{BR}(t \rightarrow H^\pm b) \times \text{BR}(H^\pm \rightarrow cb)$.

3.3 Constraints on $qb \rightarrow H^\pm \rightarrow qb$

Dedicated searches for a charged-Higgs boson where light quarks dominate both production and decay have not been performed by the experimental collaborations. However, since the signature of this channel is a dijet resonance, one can put limits on the couplings by recasting other searches. The most important searches for charged-Higgs with masses of the order of ~ 300 GeV look for two well separated jets with a high- p_T jet or photon from

³We thank Nicola Orlando for clarifying this point.

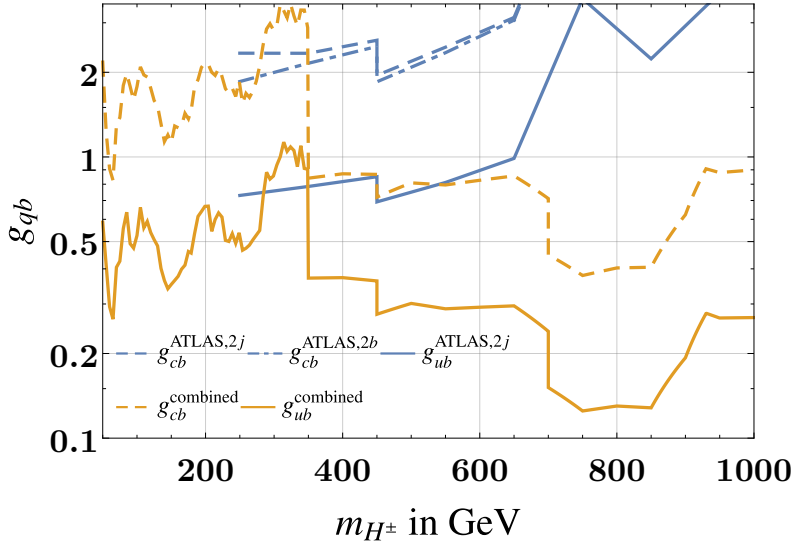


Figure 6. Upper limits at 95% CL on the couplings g_{ub} (solid) and g_{cb} (dashed) as a function of the charged-Higgs mass m_{H^\pm} from recasting Z' -searches with ISR photons in Ref. [62] (blue) and ISR jets Refs. [60, 61, 63, 64] (orange). See text for details.

initial state radiation (ISR). We have recasted these searches to obtain the limit shown in Fig. 6, which we discuss in more detail in the following.

In Ref. [62] a search has been performed for the signature $pp \rightarrow Z' \rightarrow q\bar{q}$ with an ISR photon. The selected events had been divided into two categories, one where both jets from the resonant decay are b -tagged, and the other without b -tagging. Since the resonance does not decay in two b -jets in our case, we focus on the analysis performed for the latter category⁴. However, we use the two b -tag category in the case where the resonance decays predominantly into cb , i.e. for a dominant g_{cb} coupling since the mistag rate of a charm quark is not negligible and might yield sizeable contributions in this signal region. Moreover, two different triggers have been used depending on the resonance masses and differing by the transverse energy cut on the photon $E_{T,\text{trig}}^\gamma$, and the p_T cut on the jets. The single-photon trigger, used for resonance masses below 450 GeV, requires only a single photon with transverse energy $E_{T,\text{trig}}^\gamma > 150$ GeV. Above 450 GeV, the combined trigger is used allowing for a lower transverse energy cut on the photon $E_{T,\text{trig}}^\gamma > 75$ (85) GeV for the 2016 (2017) datasets by additionally requiring two jet candidates with each $p_{T,\text{trig}}^{\text{jet}} > 50$ GeV. Photons are collected in the region $|\eta| < 2.37$ excluding $1.37 < |\eta| < 1.52$. The selection criteria are listed in Tab. 1. Additionally, if a reconstructed jet is not well separated from the isolated high- p_T photon, i.e. an angular separation of $\Delta R < 0.4$, the jet candidate is removed.

We generate $pp \rightarrow \gamma H^\pm (\rightarrow qb)$ in the five-flavor-scheme (5FS) in MadGraph5_aMC@NLO

⁴It would be interesting if the experimental search would also include a *single* b -tagged category, which would presumably give the best sensitivity to our signature as SM background is further reduced (cf. Ref. [52]). For searches that also require an ISR jet, it could be beneficial to additionally require that this ISR jet to be b -tagged, in order to reduce the background even further.

Criterion	Single-photon trigger	Combined trigger
Number of jets		$n_{\text{jets}} \geq 2$
Number of photons		$n_{\gamma} \geq 1$
Leading photon	$E_T^{\gamma} > 150 \text{ GeV}$	$E_T^{\gamma} > 95 \text{ GeV}$
Leading, subleading jet	$p_T^{\text{jet}} > 25 \text{ GeV}$	$p_T^{\text{jet}} > 65 \text{ GeV}$
Centrality	$ y^* = y_1 - y_2 /2 < 0.75$	
Invariant mass	$m_{jj} > 169 \text{ GeV}$	$m_{jj} > 335 \text{ GeV}$
Jet $ \eta $	$ \eta^{\text{jet}} < 2.8$	

Table 1. Selection criteria of Ref. [62]. Here y_1 and y_2 denote the rapidities of the leading and subleading jet (in p_T). See text for the other definitions.

at leading order using the 2HDM model file given in Ref. [72]. To populate the phase space with sufficient events fulfilling the E_T^{γ} cut on the photons, the events are generated with a p_T^{γ} cut of $p_T^{\gamma} > 100$ (50) GeV for the single-photon (combined) trigger. The analysis is performed in PYTHIA 8.2 [73, 74], and we have validated our code by applying it to the signature $pp \rightarrow \gamma Z' (\rightarrow q\bar{q})$ and comparing to the analysis by the ATLAS collaboration in Ref. [62], finding excellent agreement (cf. Appendix A). To set the limits on the charged-Higgs couplings, we calculate the local significance $Z \approx S/\sqrt{S+B}$ around the resonance, using the observed data from Ref. [62] provided in the online repository HEPData, with the number of signal events S and background events B . The resulting upper limits on the charged-Higgs couplings at 95% CL are shown in Fig. 6 in blue for g_{ub} (solid) and g_{cb} (dashed).

As it can be seen from this figure, the ISR photon search yields the most stringent constraints in the mass window between 300 and 350 GeV. Interestingly, the two b -tag category yields slightly stronger bounds for g_{cb} than the category without b -tagging, due to the moderate mistag rate of charm quarks. Below 300 GeV the strongest bounds come instead from a dijet search with an ISR jet where the two jets stemming from the resonance decay have been reconstructed as one large-radius jet [63]. Above 350 GeV the experiments usually look for two well-separated jets where the strongest constraints for masses up to 450 GeV again come from searches with an ISR jet [64]. For even higher masses the generic dijet searches yield the strongest bounds [60, 61], where for masses $\lesssim 1$ TeV only partial event informations are usually collected in order to not saturate the trigger. The ATLAS search [60] gives the strongest limits for masses below ≈ 930 GeV, while the CMS search [61] yields stronger limits for even higher masses.

In Fig. 6 we have combined all these constraints and show the strongest one in orange, which is obtained by recasting the experimental searches for a “leptophobic” Z' vector boson coupling with universal couplings to quarks in Refs. [60, 61, 63, 64]. For large resonance masses > 450 GeV, we only apply the appropriate rescaling with the parton distribution functions (PDFs). For low mass resonances we also include the efficiency ratios for Z' - and H^{\pm} -mediated events, respectively, since here deviations from the PDF-rescaling can be large due to the presence of an additional ISR jet yielding sizeable contributions

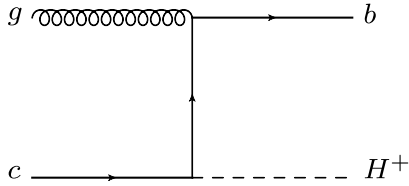


Figure 7. Charged Higgs production through gc fusion contributing to $pp \rightarrow bH^\pm$.

from gq -fusion, see e.g. Ref. [51].

3.4 Constraints on $qb \rightarrow H^\pm \rightarrow tb$

The associated production of a charged-Higgs with a single b -quark (see Fig. 7) with the subsequent decay $H^\pm \rightarrow tb$ has not been considered by the experimental collaborations, so currently there is no dedicated analysis. The authors of Ref. [48] have proposed a search for the $cb \rightarrow H^\pm \rightarrow tb$ topology based on a signature with three b -tagged jets plus lepton, which is similar to the searches in Refs. [57, 58]. In the following we will revisit the proposed analysis⁵, and extend it by **i**) studying also the case of ub production, **ii**) including the impact of systematic uncertainties and **iii**) exploring a more refined cut strategy (also employing a BDT algorithm) to further optimize the expected sensitivity.

Before explaining the details of the proposed search, we note that possible constraints on this topology could be derived by similar searches targeting a charged Higgs decaying into tb but produced via a different channel. Specifically, in Ref. [58] one signal category is focused on a resonantly produced (through light quarks) charged Higgs boson with the subsequent decay into tb . However, this signature has only been analysed for charged Higgs masses $\gtrsim 800$ GeV due to the high QCD-jet background. In order to reduce the large background and extend the search down to lower masses, one could require an additional hard b -jet in the final state. This results effectively in a three b -tagged jets plus lepton signature. One of the signal category of [57] (targeting tb production and tb decay) actually requires three b -tagged jets and one lepton, but also additional hard jets, and the resulting signal efficiency for our production mode is too small to give any relevant constraint.

We now proceed in describing the proposed search for the $qb \rightarrow H^\pm \rightarrow tb$ topology. The basic selection requires events with at least three b -tagged jets and one lepton (e or μ) with transverse momenta of $p_T^b > 20$ GeV and $p_T^l > 30$ GeV, respectively. Moreover, events are required to have missing energy of $E_T^{\text{miss}} > 35$ GeV. The angular separation ΔR between any two b -jets and between any b -jet and the lepton should satisfy $\Delta R > 0.4$. Furthermore, a pseudo-rapidity cut of $|\eta| < 2.5$ is applied to the lepton and all b -jets. Finally, the sum H_T of the transverse momenta of the three b -jets and the lepton momentum should satisfy $H_T > 350$ GeV. The dominant background is $t\bar{t}$ production, which we have simulated in MadGraph5_aMC@NLO with up to two additional jets in the five-flavour scheme. In the same way we generate the signal $pp \rightarrow H^\pm(\rightarrow tb) + js$ with up to two additional jets in the five-flavour scheme using the 2HDM model file provided in Ref. [72].

⁵We thank the authors of Ref. [48] for correspondence about their results.

The resulting Les Houches Event (LHE) file is fed into a PYTHIA 8.2 standalone version. Jets are matched using the MLM jet matching algorithm [68, 75, 76]. The jet finding is performed with FastJet [77, 78] using the anti- k_T algorithm with a radius parameter of $R = 0.6$. The K factor is determined by dividing the NNLO cross section, see Ref. [79] and references therein, by the leading order cross section after jet merging. This yields $K \approx 1.6$. We implement jet tagging as follows: the closest jet (within a given radius ΔR) to a b -quark that originates from the initial hard process is marked as a b -jet, and similarly the closest jet to a c -quark that originates from initial hard process is marked as a c -jet. Every other jet are potential mistag candidates, with an assigned mistagging probability taken from the Delphes detector cards that use the operating point of Ref. [80] with 70% b -tagging probability. Similarly b - and c -jets are identified as such by multiplying with a tagging probability. We have validated our PYTHIA code (in particular the jet tagging algorithms) by comparing to the simulations obtained for similar signatures by ATLAS [81] and CMS [82], for which we obtain excellent agreement (see Appendix B for details).

Our results for the LO partonic cross sections are given in Tab. 2 for a benchmark point with $g_{tb} = 0.6$, $g_{cb} = 0.4$, $m_{H^\pm} = 300$ GeV. This choice corresponds to the benchmark point “BP1” in Ref. [48], and we essentially agree on the values for signal and dominant background ($t\bar{t} + \text{jets}$), although we find small discrepancies for sub-leading backgrounds.

	$t\bar{t} + 2j$	$Wt + 2j$	$tj + 1j$	$t\bar{t}h$	$t\bar{t}Z$	$2j + H^\pm \rightarrow tb$
$\sigma_{\text{had}}^{\text{inclusive}}$	614 pb	72 pb	218 pb	480 fb	709 fb	28 pb
n_{events}	34567910	37350	383497	10000	10000	133247
$\geq 3j, p_T^b, \eta_b$	33535695	34901	301202	9973	9925	116646
$\geq 3b$	1425532	815	4040	2849	1097	10946
ΔR_{bb}	1425532	815	4040	2849	1097	10946
η_l	1258837	708	3311	2722	1030	9496
$p_T^{l,\text{veto}}$	776939	427	1493	2026	745	5278
$\Delta R_{lb}, p_T^l$	228213	131	180	675	257	1036
exactly 1 lepton	210654	119	176	534	218	1020
E_T^{miss}	143130	74	104	363	155	630
H_T	45184	25	23	181	76	71
$\sigma_{\text{had,LO}}$ [fb]	802 ± 4	49 ± 10	13 ± 3	8.7 ± 0.6	5.4 ± 0.6	14 ± 2

Table 2. Cutflow of leading order partonic cross sections after merging in the 5FS.

In order to study the experimental sensitivity of the proposed analysis, we have used our PYTHIA code to perform a “cut and count” analysis, and calculate the statistical significance Z according to $Z \approx S/\sqrt{S+B+(\epsilon B)^2}$, with the number of signal events S , background events B and relative systematic background uncertainty ϵ . This analysis is performed for each charged-Higgs mass point, calculating the number of signal events as a function of the couplings g_{tb} and g_{cb} by a simple rescaling. In this way one can calculate

the expected⁶ 95% CL exclusion limits in the plane of couplings for a given Higgs mass, and we show the exclusion curves for $m_{H^\pm} = 300, 500, 750, 1000$ GeV in the left panel of Fig. 8.

In the same way we can calculate exclusion curves on the product $g_{tb}g_{ub}$, shown in the right panel of Fig. 8. These limits are stronger simply because of the larger parton luminosities for up-quarks as compared to charm quarks, which control charged Higgs production through ug (cg) fusion. Note that for large g_{tb} the contribution to charged Higgs production from associated production with top quarks is not negligible anymore, and the constraints from the proposed analysis no longer apply. We therefore indicate with a hatching the region where associated production with top quarks makes up more than 10% in both panels of Fig. 8.

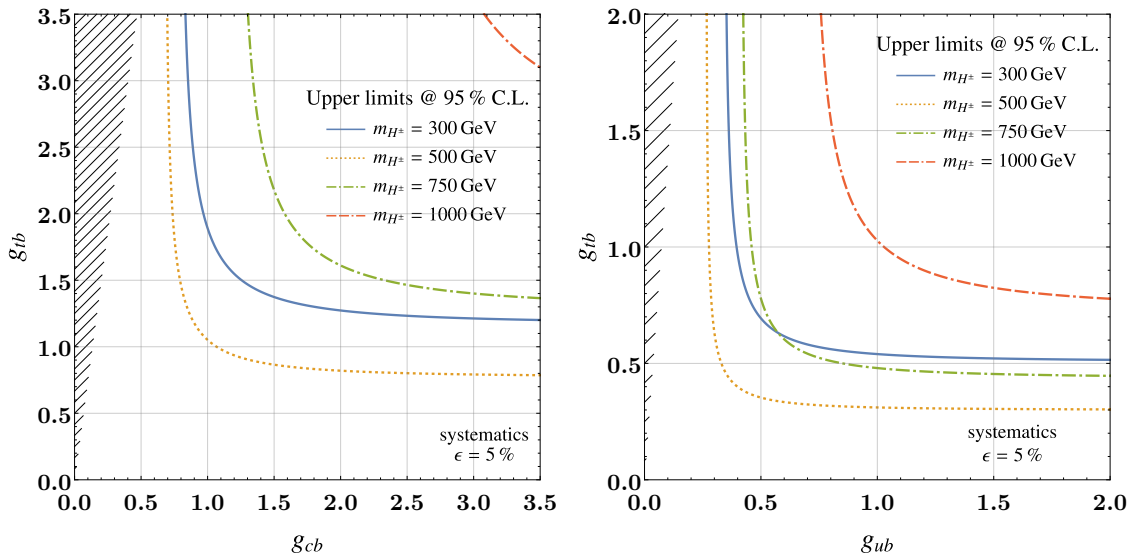


Figure 8. Expected 95% CL upper limits in the plane of charged Higgs couplings g_{tb} - g_{cb} (left panel) and g_{tb} - g_{ub} (right panel) for different charged-Higgs masses and $\sqrt{s} = 14$ TeV @ 139 fb⁻¹. When the ratio of g_{tb}/g_{cb} (g_{tb}/g_{ub}) becomes so large that charged Higgs production is no longer dominated by ug (cg) fusion, the bounds from the proposed analysis lose their validity. We indicate this region, roughly defined when associated production with top quarks makes up more than 10% of total charged Higgs production, with a hatching.

We also provide the constraints on the product of production cross section and branching ratio in Fig. 9. The dashed line indicates the 95% CL_s limits that can be obtained if only background was observed, while the green (yellow) bands are the projected 95% CL_s limits corresponding to up- and downward fluctuations of the background at 68% (95%).

⁶That is the limits one could obtain if only background was observed.

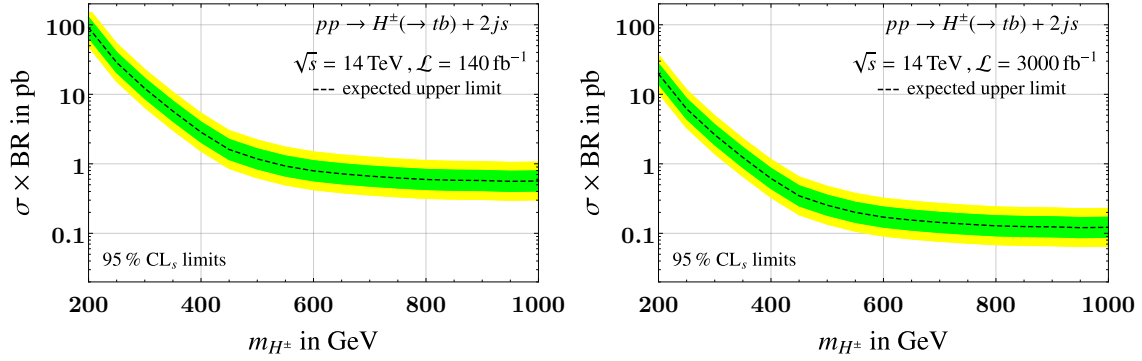


Figure 9. Expected upper limits at 95% CL_s on the production cross section times branching ratio $\sigma(gq \rightarrow bH^\pm) \times \text{BR}(H^\pm \rightarrow tb)$ as a function of the charged Higgs mass. Shown in green (yellow) are the projected limits corresponding to background fluctuations of 68% (95%).

Finally, we demonstrate that the sensitivity can be further improved by optimizing the baseline cuts proposed in Ref. [48]. We take the same basic signal region, i.e. ≥ 3 b -jets with $p_T \geq 20$ GeV and exactly 1 lepton with $p_T \geq 30$ GeV, all satisfying $|\eta| < 2.5$, and vary the cuts on missing transverse energy E_T^{miss} and total transverse momentum $H_T = p_T^l + \sum_{i=1}^3 p_T^{b_i}$.

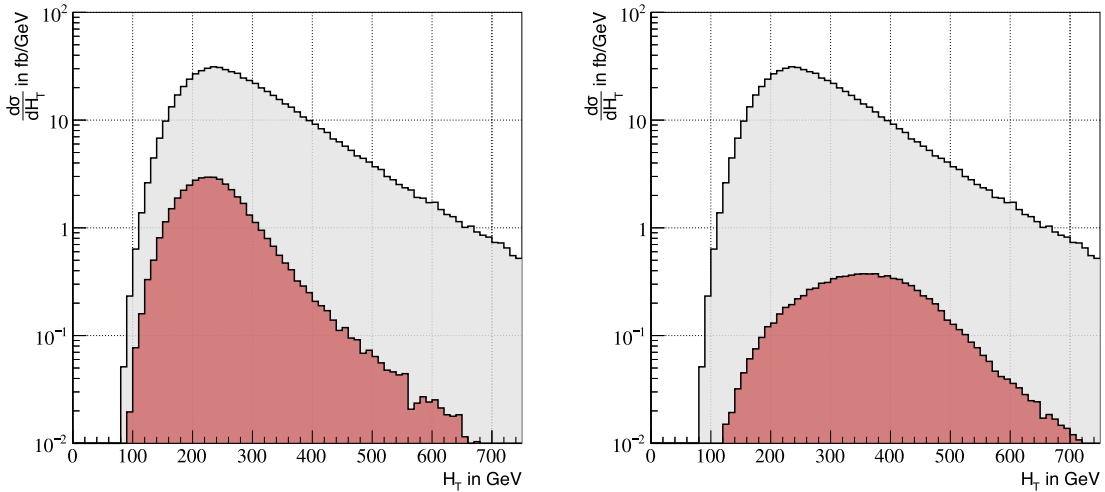


Figure 10. Binned differential cross-section in the signal region for $g_{tb} = 0.6, g_{cb} = 0.4$ and $\sqrt{s} = 14 \text{ TeV} @ 140 \text{ fb}^{-1}$, as a function of the sum of transverse momenta H_T for $m_{H^\pm} = 300 \text{ GeV}$ (left panel) $m_{H^\pm} = 500 \text{ GeV}$ (right panel).

As can be seen from the histograms in Fig. 10, a cut on H_T can be helpful in distinguishing signal and background for Higgs masses above 500 GeV (we have checked that a cut on E_T^{miss} has less impact). In the following we consider two procedures to maximize the significance $Z \approx S / \sqrt{S + B + (\epsilon B)^2}$: we try to strengthen the single cuts on p_T, H_T

and E_T^{miss} by hand (“optimized cuts”), and also employ a boosted-decision-tree (BDT) algorithm to find the best cuts (“BDT”), see Appendix C for more details. We apply these procedures to the couplings of the benchmark scenario BP1 ($g_{tb} = 0.6, g_{cb} = 0.4$), and take as a reference point the basic cuts for $m_{H^\pm} = 300$ GeV, $H_T > 350$ GeV and $E_T^{\text{miss}} > 35$ GeV. In Fig. 11 we calculate the sensitivity for 140 fb^{-1} as a function of the charged Higgs mass for this reference point (shown in blue). This is compared to an analysis with additional cuts (in green) and the optimized BDT analysis (in orange). We take into account systematic errors through the parameter ϵ , and show results for the cases $\epsilon = 5\%$ (left panel) and $\epsilon = 10\%$ (right panel). As one can see from this figure the optimized cuts allow a slight gain of sensitivity for Higgs masses above 500 GeV, while the BDT can potentially increase the sensitivity by an order of magnitude, even for small Higgs masses. We expect that a realistic analysis gives sensitivities that fall between our analyses with additional cuts and the BDT (i.e. between orange and green points in Fig. 11), provided that we did not underestimate systematic errors.

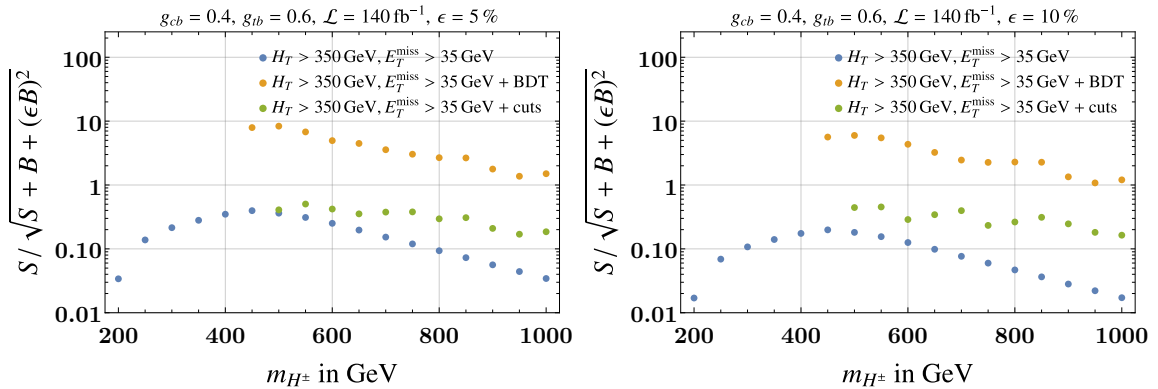


Figure 11. Significance Z as a function of the charged Higgs mass for various cuts. Shown are results for a systematic error of $\epsilon = 5\%$ (left panel) and $\epsilon = 10\%$ (right panel). Blue points correspond to the cuts of BP1 in Ref. [48], green ones to additional cuts on p_T, H_T and E_T^{miss} , and orange points correspond to optimised cuts using a boosted-decision-tree algorithm (BDT).

3.5 Charge asymmetry

In this subsection we explore the possibility of employing charge asymmetry information to further probe at the LHC a charged Higgs with flavour violating couplings in the $qb \rightarrow H^\pm \rightarrow tb$ channel. Previous studies on charge asymmetries, focussing on the opportunity to use this variable to detect single top signatures or new physics models, include Refs. [83–89].

For a specific final state including one reconstructed lepton, a charge asymmetry variable \mathcal{A}_C can be constructed as

$$\mathcal{A}_C = \frac{N_+ - N_-}{N_+ + N_-} \quad (3.1)$$

where N_+ (N_-) denote the number of events with positive (negative) charged lepton. As we will briefly review in the following, the advantage of using this variable for setting limits

(or improving discovery potential) is that many systematic uncertainties simplify in this ratio.

The uncertainty on the charge asymmetry \mathcal{A}_C is calculated using the usual variance formula for independent variables. In this case, the total statistical uncertainty $\delta_{\mathcal{A}_C}^{\text{stat}}$ simplifies to

$$\delta_{\mathcal{A}_C}^{\text{stat}} = 2\sqrt{\frac{N_+ N_-}{(N_+ + N_-)^3}}, \quad (3.2)$$

since N_+ and N_- are Poisson distributed. Also a total systematic uncertainty $\delta_{\mathcal{A}_C}^{\text{syst}}$ arises from combining the systematic uncertainties on all processes p_i that yield a non-vanishing charge asymmetry $\mathcal{A}_C(p_i)$

$$\delta_{\mathcal{A}_C}^{\text{syst}} \approx \frac{\sqrt{\sum_i \left[\delta_{\sigma(p_i)}^2 (\mathcal{A}_C^2(p_i) + \mathcal{A}_C^2) \right]}}{\sum_i \sigma(p_i)}, \quad (3.3)$$

where $\delta_{\sigma(p_i)}$ denotes the systematic uncertainty on the production cross section of the process p_i . Note that the first term, which arises from the uncertainty on $N_+ - N_-$, typically dominates over the second term that arises from propagating the uncertainty on $N_+ + N_-$.

In the case of a charged Higgs coupled predominantly to either ub or cb and the corresponding $bb\bar{b}l$ signature, as studied in this section, the use of the charge asymmetry can be twofold. On one hand, it can be employed as a new variable to test the pure ub coupling hypothesis, since for such coupling the new physics signal is maximally charge asymmetric, contrary to the SM background. On the other hand, in the optimistic case of a signal discovery in the $bb\bar{b}l$, it can effectively discriminate between ub and cb production once restricted to the signal events.

We begin the discussion with the second application of \mathcal{A}_C , the signal discrimination. In Fig. 12 we show the charge asymmetry variable for the signal in the case of ub and cb production, for the benchmark scenario BP1 with varying charged Higgs mass, and we have also included statistical and systematic uncertainties. The ub channel is very charge asymmetric because the production mode involves a valence quark. Note that the value of the coupling is not relevant for the central value of the asymmetry, but the overall cross section will modify the number of events and hence will impact the statistical error. We conclude that the ub and cb production can be easily discriminated by using the charge asymmetry variable \mathcal{A}_C for a sufficient number of observed events.

We proceed by analyzing the constraining potential of the charge asymmetry variable in the case of pure ub coupling. In this case \mathcal{A}_C can be useful since the main background is $t\bar{t}$ production, which is mainly charge symmetric. Indeed only the interference between $q\bar{q}$ -initiated processes at NLO and LO yields a negative value of $\mathcal{A}_C^{t\bar{t}}$ (that gets smaller for increasing rapidity cut), while the main contribution to the $t\bar{t}$ cross-section comes from gluon fusion that is charge symmetric to all orders [84, 90]. Contributions to the charge asymmetry from qg and $\bar{q}g$ fusion are subleading.

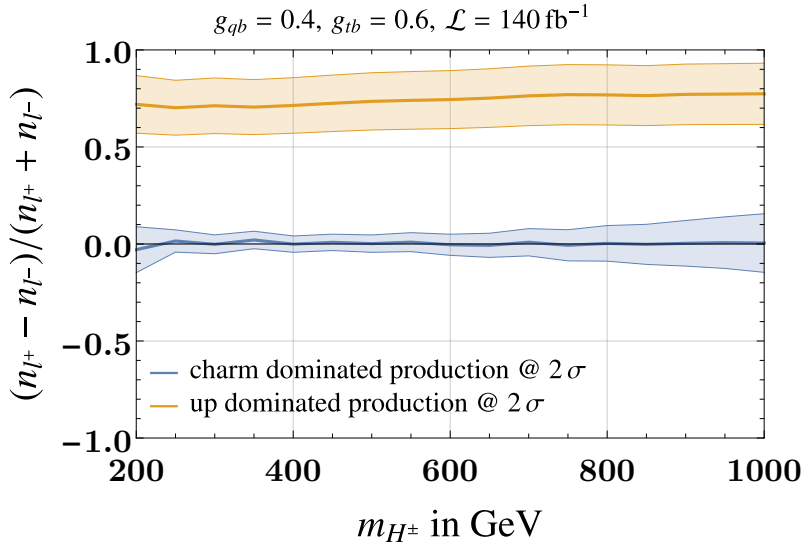


Figure 12. Charge asymmetry for the charged Higgs signature (in $bbb\ell$) for the cases of pure ub (orange) or cb (blue) production, as a function of the charged Higgs mass. The production through the ub coupling displays a significant charge asymmetry due to the initial state valence quark. We also display combined statistical and systematic uncertainties, with the latter assumed to be 10%.

In order to estimate the discovery potential of the charge asymmetry variable, we evaluate it for the case of only SM and for SM+charged Higgs signal, fixing the ub coupling to a representative value. In case of the SM, we also take into account the subleading contributions from single-top production besides the main $t\bar{t}$ background which is the most relevant one after the $bbb\ell$ selection, cf. Tab. 2. The single-top backgrounds have to be taken into account since the uncertainty on their cross-sections can have a sizeable effect on the error estimate due to $\mathcal{A}_C^{\text{single-top}} \approx 1/3$, see Eq. (3.3). We estimate the uncertainties by adding statistical uncertainty and a systematic uncertainty of 100% (single-top) and 200% ($t\bar{t}$) on the SM backgrounds. The latter error (which we actually deem to be conservative [84, 85]) reflects the fact that we are only partially taking into account the NLO contribution to \mathcal{A}_C from $t\bar{t}$ production, as we are not considering QCD loop corrections that are mainly responsible for the charge asymmetry in the SM.

The resulting uncertainty band is shown in Fig. 13. Within these assumptions, the charge asymmetry variable can for instance exclude a charged Higgs with ub coupling $g_{ub} = 0.4$ in the mass range $325 \text{ GeV} \lesssim m_{H^\pm} \lesssim 575 \text{ GeV}$. While a detailed quantitative investigation of the systematic uncertainties in the measurement of \mathcal{A}_C is beyond the scope of this paper, our analysis demonstrates that the use of charge asymmetry variables can provide a promising complementary test of this new physics signature.

4 Constraints on Charged Higgs Couplings

In this section we summarize the constraints on charged Higgs couplings to b -quarks defined in Eq. (1.1), combining the flavor constraints from Section 2 and the collider constraints

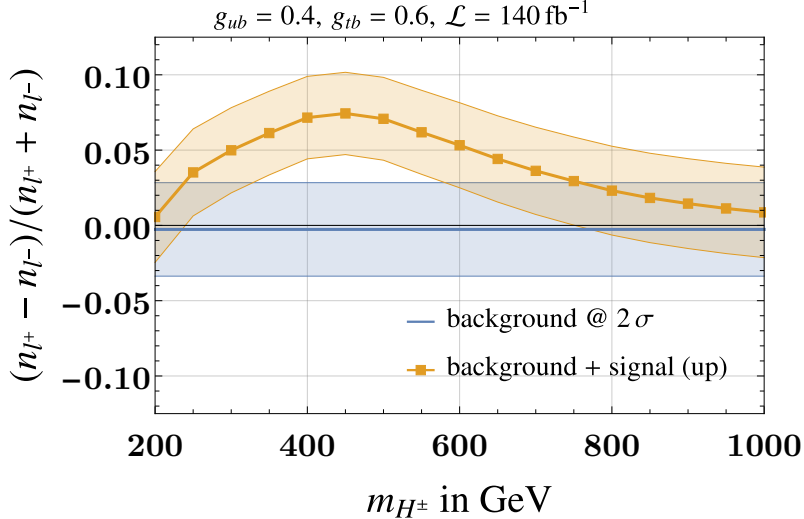


Figure 13. Charge asymmetry comparison between the signal (charged Higgs production through the ub coupling) and the SM background, as a function of the charged Higgs mass, for the final state selection $bbbl$ explained in the text. We include statistical and systematic uncertainties in the SM estimate of the asymmetry, see text for details.

for the various production and decay topologies from Section 3.

If a single coupling dominates, the constraints are trivially given by Figs. 4 and 5 for dominant g_{tb} coupling, and Fig. 6 for dominant g_{cb} or g_{ub} coupling. We summarize these constraints in Fig. 14.

If both g_{ub} and g_{cb} are sizable, the bounds from flavor physics (cf. Fig. 2) and dijet searches (cf. Fig. 6) are complementary, as seen in Fig. 15, where these constraints have been overlaid in the $g_{ub}-g_{cb}$ -plane for two choices of the charged Higgs mass. While for low Higgs masses the flavor constraints dominate for couplings of similar size, these constraints quickly fade for larger Higgs masses, while instead the dijet searches become more effective. Note that in the limit where a single coupling dominates the limits in Fig. 14 are recovered, but generically the bounds are stronger because the two production channels add up.

At present there is no experimental search that specifically probes the non-trivial interplay of top and light quark couplings. However, as discussed in Section 3.4, strong bounds can be obtained already with present data if dedicated searches for the $qb \rightarrow H^\pm \rightarrow tb$ signature are carried out, as shown in Fig. 8. We overlay the expected constraints with the limits on single couplings in Fig. 16 (Fig. 17), which summarizes all relevant bounds in the plane $g_{cb}-g_{tb}$ ($g_{ub}-g_{tb}$) for 140 fb^{-1} and two choices for the charged Higgs mass. The grey regions indicate the limits from single coupling searches, either from dijet searches for dominant qb coupling (cf. Fig. 6), or the usual searches for top charged Higgs production and decay for dominant tb coupling (cf. Fig. 4). Note that these bounds are loosened when the non-dominant coupling is increased, simply due to the reduction of the relevant branching ratio.

The red contours instead indicate the parameter space that could be probed by the

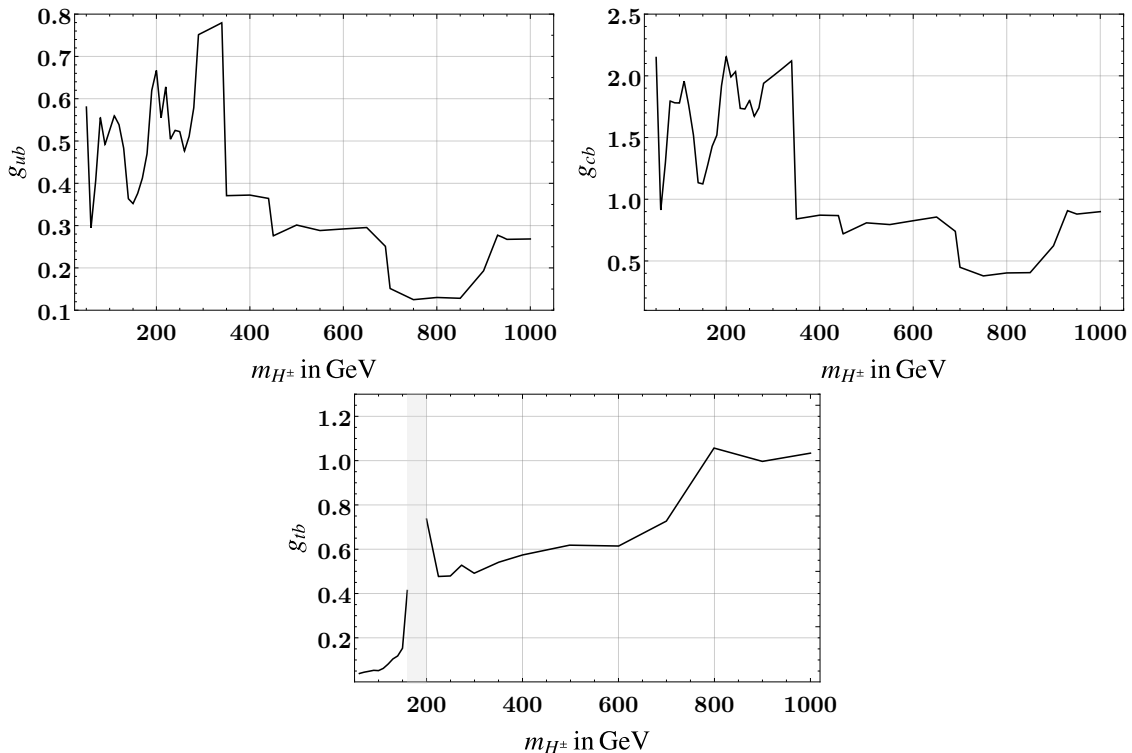


Figure 14. Combined constraints on charged Higgs couplings in the limit where the coupling g_{ub} (left upper panel), g_{cb} (right upper panel) or g_{tb} (lower panel) dominates.

dedicated search for $qb \rightarrow H^\pm \rightarrow tb$ as discussed in detail in Section 3.4. Dashed red lines show the sensitivity for simple cuts on top of $H_T > 350$ GeV, $E_T^{\text{miss}} > 35$ GeV, while the solid red line denote the constraints we obtained from cut optimization used a BDT algorithm. We expect that a realistic analysis carried out by the experimental collaborations will yield constraints between these two curves, and thus has the potential to substantially improve present bounds, in particular for light Higgs with couplings to ub and cb quarks of similar size. Therefore such searches will probe a significant portion of previously uncharted parameter space, which can be seen from Fig. 18, where we show the same lines as in Figs. 16 (Fig. 17), but in the plane $m_{H^\pm} - g_{cb}$ ($m_{H^\pm} - g_{ub}$) for fixed coupling $g_{tb} = 0.6$. This figure also shows that using the BDT is roughly equivalent to reducing the systematic uncertainties by 5%.

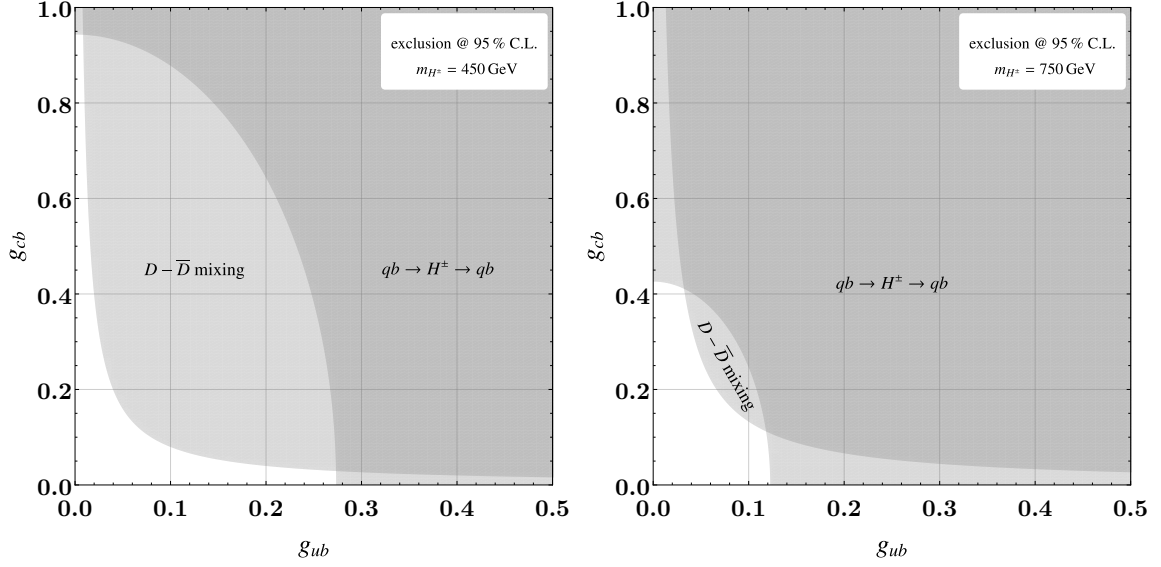


Figure 15. Present 95% CL constraints in the coupling plane $g_{ub}-g_{cb}$ for $m_{H^\pm} = 450$ GeV (left panel) and $m_{H^\pm} = 750$ GeV (right panel). Shown are the constraints from dijet searches [60, 61, 63, 64] denoted by “ $qb \rightarrow H^\pm \rightarrow qb$ ” and flavor constraints denoted by “ $D-\bar{D}$ mixing”.

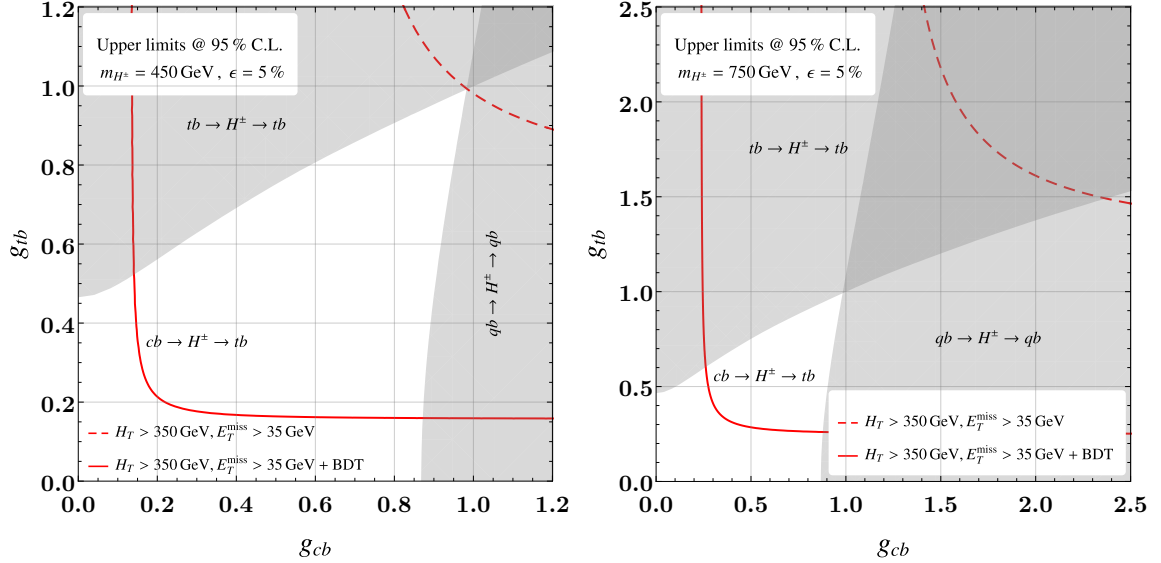


Figure 16. Expected 95% CL upper limits in the coupling plane $g_{cb}-g_{tb}$ for 140 fb^{-1} and charged Higgs masses of 450 GeV (left panel) and 750 GeV (right panel). Shown are the constraints from single coupling searches based on dijet searches [62] denoted by “ $qb \rightarrow H^\pm \rightarrow cb$ ”, and searches for top charged Higgs production and decay [57] denoted by “ $tb \rightarrow H^\pm \rightarrow tb$ ”. The red lines denoted by “ $cb \rightarrow H^\pm \rightarrow tb$ ” indicate the parameter space that could be probed by the search described in Section 3.4. The dashed red line shows the constraints from applying the indicated cuts, while the solid line shows the constraints obtained from optimized cuts using a BDT algorithm. We assume a systematic uncertainty of 5%.

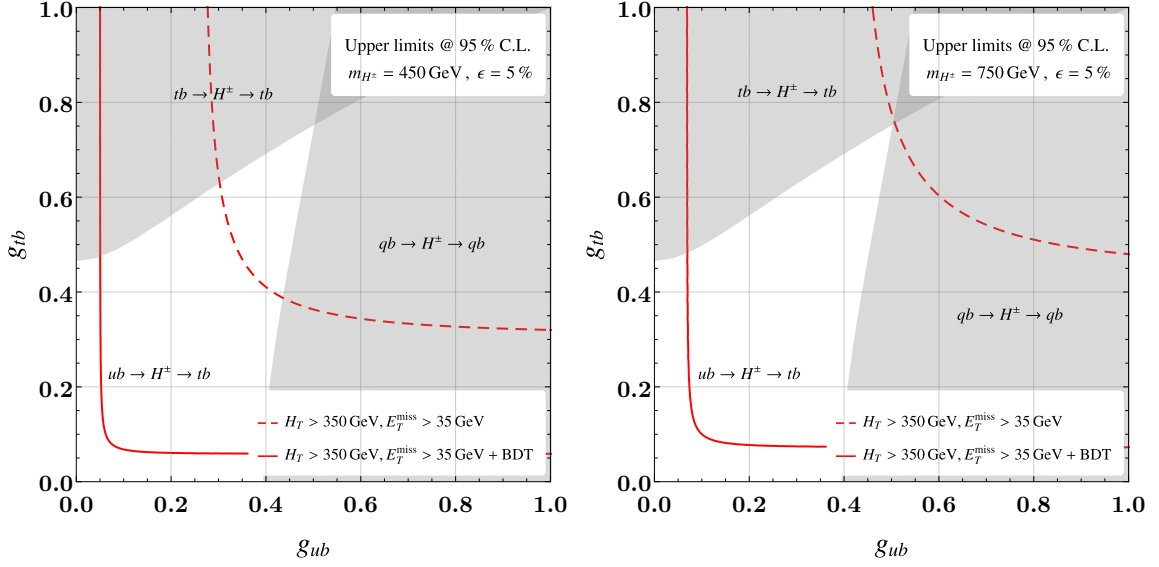


Figure 17. As Fig. 16, but for the coupling g_{ub} instead of g_{cb} .

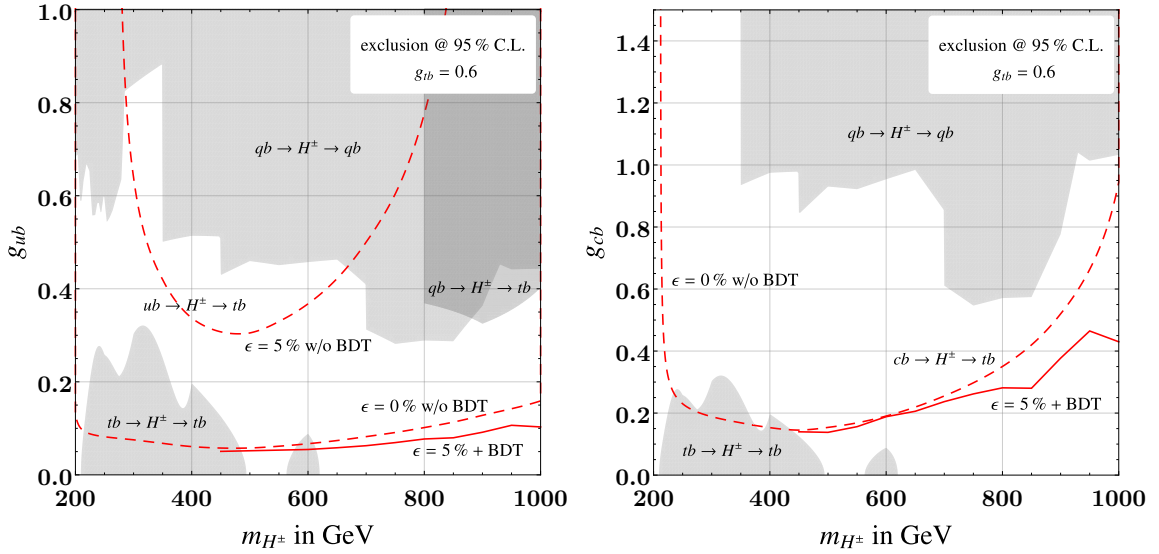


Figure 18. Expected 95% CL exclusion limits in the plane m_{H^\pm}/g_{ub} (left panel) and m_{H^\pm}/g_{cb} (right panel) for fixed $g_{tb} = 0.6$. Shown in gray are the constraints from single coupling searches based on dijet searches [62] denoted by “ $qb \rightarrow H^\pm \rightarrow qb$ ”, searches for top-associated charged Higgs production and decay [57] denoted by “ $tb \rightarrow H^\pm \rightarrow tb$ ”, and the constraints from resonant charged Higgs production decaying into tb [58] denoted as “ $qb \rightarrow H^\pm \rightarrow tb$ ”. The latter are relevant only for g_{ub} and large Higgs masses. The red lines indicate the parameter space that could be probed by the search described in Section 3.4, denoting the constraints from applying the cuts in Fig. 16 with (solid) or without BDT optimization (dashed), for different assumed systematic errors ϵ .

5 Summary and Conclusions

In this work we have systematically studied model-independent constraints on generic charged Higgs couplings to b -quarks. Flavor physics (D -meson mixing and flavor-violating top decays) gives only weak constraints, so that LHC searches play a crucial role in probing these couplings. So far ATLAS and CMS have performed dedicated searches only for charged Higgses that dominantly couple to tb quarks, resulting in constraints that we summarize in Fig. 14 (lower panel). If instead couplings to ub or cb quarks dominate, one can recast existing dijet searches for leptophobic Z' fields in order to obtain the bounds in the upper panels of Fig. 14. These constraints could be strengthened by new dedicated searches in the following way:

- Looking for light charged Higgses produced from top decays $t \rightarrow bH^\pm(\rightarrow ub)$ in a similar way to the existing search for $t \rightarrow bH^\pm(\rightarrow cb)$, see Section 3.2.
- Extending the dijet searches for Z' vector bosons also with *single* b -tagging, in order to improve sensitivity on scenarios with flavor-violating couplings, see Section 3.3.

If couplings to both ub and cb quarks are sizable, there is a non-trivial interplay between LHC searches and flavor physics. Dijet searches are actually complementary to flavor physics, see Fig. 15, as the latter give constraints that quickly decouple with the charged Higgs mass, while the former gain sensitivity for heavy Higgses when hard cuts on transverse jet momenta can significantly reduce SM background.

Up to now there have been no dedicated searches that look for a charged Higgs that has sizable couplings to both qb and tb quarks. We have discussed in detail how one can profit from their interplay in order to significantly extend the existing reach on the parameter space from single coupling constraints alone, see Fig. 16, Fig. 17 and Fig. 18. Specifically we have proposed two new search strategies:

- Probing the top decay channels $qb \rightarrow H^\pm \rightarrow tb$ using multi- b -jet signatures similar to Ref. [57], but with lower (b -)jet multiplicity, see Section 3.4.
- Employing charge asymmetries that allow to both distinguish c - and u -production in $qb \rightarrow H^\pm \rightarrow tb$ and reduce SM background, see Section 3.5.

In summary we think it is worthwhile to develop and carry out dedicated collider searches for all three charged Higgs couplings to b -quarks, since the reach of flavor physics is limited and present LHC searches focus on the tb coupling. We suggested various new search strategies that are mainly slight extensions of existing analyses, which hopefully are useful for experimentalists to design realistic searches that allow to boost the LHC reach on scenarios with generic charged Higgs couplings.

Acknowledgements

We thank Nicola Orlando and Syuhei Iguro for useful discussions. This work is partially supported by project C3b of the DFG-funded Collaborative Research Center TRR257,

“Particle Physics Phenomenology after the Higgs Discovery”. AM is supported by the Strategic Research Program High-Energy Physics and the Research Council of the Vrije Universiteit Brussel, and by the “Excellence of Science - EOS” - be.h project n.30820817.

A Validation of PYTHIA code used for $qb \rightarrow H^\pm \rightarrow qb$ analysis

Here we cross-check our analysis procedure which we used to recast the results of Ref. [62], cf. Section 3.3. For this we apply our code to the Z' model that has been analysed in the very same reference. This enables a direct comparison between our analysis and the experimental one. The data for the process $pp \rightarrow \gamma Z' (\rightarrow jj)$ is generated in `MadGraph5_aMC@NLO` using the vector-leptoquark model file of Ref. [91]. The acceptance of our procedure is shown together with the acceptance of the experimental analysis, that can be found in the auxiliary materials of Ref. [62], in Fig. 19. Further, we determine the limits on the coupling as described in Section 3.3. The result is shown in Fig. 19 where we overlaid the results of Ref. [62]. Both results show a good agreement with the more sophisticated experimental analysis.

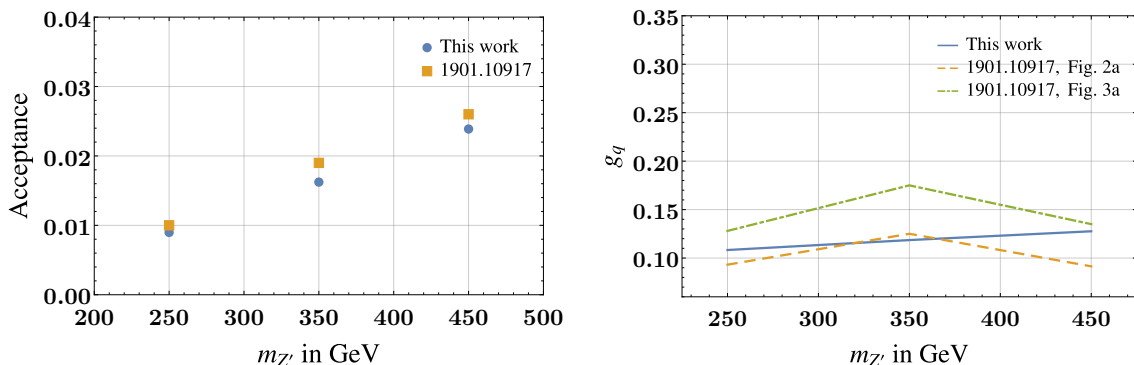


Figure 19. Comparison of the acceptance (left) and of the limit on the coupling (right) between our analysis and the experimental analysis from Ref. [62] (1901.10917).

B Validation of PYTHIA code used for $qb \rightarrow H^\pm \rightarrow tb$ analysis

In order to validate our PYTHIA code that we used for the $qb \rightarrow H^\pm \rightarrow tb$ analysis, we have used the same code to reproduce the number of simulated SM background events after cuts in various channels as obtained by the experimental collaborations in the Ref. [81] (ATLAS) and Ref. [82] (CMS).

B.1 Validation with arXiv:1209.4397 (CMS)

The CMS analysis was dedicated to the production of heavy resonances decaying into top-antitop quark pairs using 5.0 fb^{-1} at $\sqrt{s} = 7 \text{ TeV}$. SM background events from $t\bar{t}$ production were generated using `MADGRAPH 5.1.1`, `PYTHIA 6.4.24` (generating $pp \rightarrow t\bar{t}$ with up to two additional jets) and `POWHEG` event generators using `CTEQ6L` parton distribution functions of the proton. On these events selection cuts were imposed by requiring exactly one isolated

muon with $p_T^l > 30$ GeV and $|\eta^l| < 2.1$ and at least three jets with transverse momentum $p_T^j > 50$ GeV, $|\eta| < 2.5$, where the leading leading jet has at least $p_T > 70$ GeV. The anti- k_t algorithm with $R = 0.5$ was used for jet clustering, where candidates identified as leptons were excluded from jet clustering. Moreover, missing transverse energy of at least 20 GeV were required, and only tracks with transverse momentum above 0.5 GeV were taken into account. Different signal categories were obtained by varying the number of required jets and b -tagged jets. The cross sections have been normalized to the NLO values given in Ref. [82] ($\sigma_{t\bar{t}}^{7\text{TeV}} = 157.5$ pb), corresponding to a K -factor of 1.51.

In Tab. 3 we display the numbers of events which passed all cuts in the various signal categories, where e.g. “ $\geq 4j, 1b$ ” means at least four jets of which there is one b -tagged jet. Within statistical errors we find excellent agreement with the simulated events obtained by the CMS collaboration.

	$3j, \geq 1b$	$\geq 4j, 0b$	$\geq 4j, 1b$	$\geq 4j, \geq 2b$
Our analysis	7657 ± 1245	2214 ± 668	8261 ± 1294	7657 ± 1245
Ref. [82]	5612	2988	7802	6093

Table 3. Expected number of events for $t\bar{t}$ production at $\sqrt{s} = 7$ TeV and 5.0fb^{-1} obtained with our analysis code and by the CMS collaboration in Ref. [82]. For our analysis we only show the statistical errors from the limited MC samples we used, whereas the errors in the numbers of Ref. [82] are dominated by systematic uncertainties, which amount to roughly 10%.

B.2 Validation with arXiv:1512.03704 (ATLAS)

The ATLAS analysis was dedicated to the search for charged Higgs bosons produced in association with a top quark $gb \rightarrow tH^\pm$ decaying to tb using 20.3fb^{-1} at $\sqrt{s} = 8$ TeV. SM background events from $t\bar{t}$ production were simulated with Powheg-Box v2.0, using the CT10 PDF set. These events were interfaced to Pythia v6.425, with the Perugia P2011C tune for the underlying event. Events were further selected by requiring exactly one isolated lepton, satisfying $E_T > 25$ GeV, $|\eta| < 2.47$ (electrons) and $p_T > 25$ GeV, $|\eta| < 2.5$ (muons), and at least 4 jets with transverse momentum $p_T^j > 25$ GeV and pseudo-rapidity $|\eta^j| < 2.5$. The anti- k_t algorithm with $R = 0.4$ was used for jet clustering, where candidates identified as leptons were excluded from jet clustering. Moreover, missing transverse energy of at least 20 GeV were required, and only tracks with transverse momentum above 0.5 GeV were taken into account. The b -tagging algorithm has 70% efficiency to tag a b -quark jet, with a light-jet mistag rate of 1% and a c -jet mistag rate of 20%. The $t\bar{t}$ cross sections have been normalized to the NNLO values given in Ref. [81] ($\sigma_{t\bar{t}}^{8\text{TeV}} = 253$ pb), corresponding to a K -factor of 1.72.

In Tab. 4 we display the numbers of events which passed all cuts in the various signal categories, where e.g. “ $\geq 4j, 3b$ ” means at least four jets of which there are three b -tagged jet. Within statistical errors we find excellent agreement with the simulated events obtained by the ATLAS collaboration.

	$4j, 2b$	$5j, 2b$	$\geq 6j, 2b$	$4j, \geq 3b$	$\geq 5j, \geq 3b$
Our analysis	71508 ± 3142	41654 ± 2374	28631 ± 1990	5063 ± 838	8624 ± 1082
Ref. [81]	87220 ± 13740	44750 ± 10830	24490 ± 8420	7700 ± 1780	9700 ± 3800

Table 4. $t\bar{t}js$: Expected number of events for $t\bar{t}$ production at $\sqrt{s} = 8$ TeV and 20.3 fb^{-1} obtained with our analysis code and by the ATLAS collaboration in Ref. [81]. For our analysis we only show the statistical errors from the limited MC samples we used, whereas the errors Ref. [81] are dominated by systematic uncertainties.

C BDT analysis of $qb \rightarrow H^\pm \rightarrow tb$ signature

In order to maximise the reach of the search, we perform a multivariate analysis by employing a boosted-decision-tree (BDT). For this, we use an AdaBoost classifier as implemented in the `scikit-learn` library in Python. For Higgs masses below (equal and above) 800 GeV, we train the classifier using 10 trees and a learning rate of 0.4 with each tree having a maximal depth of 14 (8).

The BDT is trained on 10^5 unweighted $t\bar{t}$ background events and 10^4 unweighted signal events which have passed the selection region defined as

$$p_T^j > 20 \text{ GeV}, \quad p_T^l > 30 \text{ GeV}, \quad H_T > 350 \text{ GeV}, \quad E_T^{\text{miss}} > 35 \text{ GeV}, \quad |\eta| < 2.5, \quad (\text{C.1})$$

with exactly one lepton and at least three b -jets, cf. Section 3.4 The variables included in the training are

- $p_{T,i}^b$ of the three leading b -jets, $i = 1, 2, 3$
- p_T^l of lepton
- scalar sum of the p_T of the three b -jets and lepton
- missing energy E_T^{miss}
- ΔR between the three leading b -jets and the lepton, denoted as R_{ij}^b and R_{li} for the distance between the i th and j th b -jet, and the i th b -jet and lepton, respectively
- pseudo-rapidity of the three leading b -jets η_i^b and the lepton η^l
- number of jets n_{jets}
- number of b -jets $n_{b\text{-jets}}$

Note that the BDT is only trained on the signal events and the dominant $t\bar{t}$ background, however, the performance evaluated with a separate dataset for a luminosity of $\mathcal{L} = 140 \text{ fb}^{-1}$ takes into account all processes listed in Tab. 2. We show the results exemplary for the 450 GeV charged-Higgs mass point with $g_{cb} = 0.4$ and $g_{tb} = 0.6$ and a systematic uncertainty of $\epsilon = 5\%$. The receiver operating curve showing the true positive over false positive

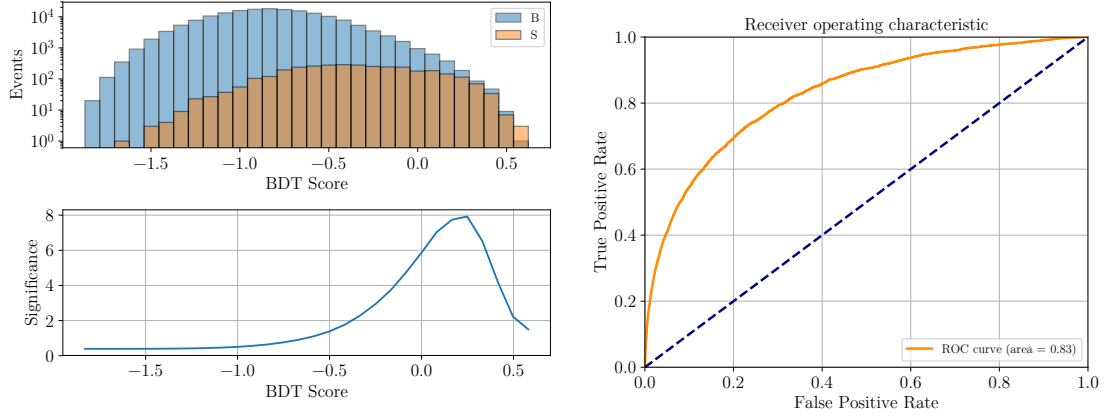


Figure 20. $\mathcal{L} = 140 \text{ fb}^{-1}$. *Left:* Significance $Z \approx S/\sqrt{S + B + (\epsilon B)^2}$ for $\epsilon = 5\%$ as a function of the BDT cut. *Right:* Receiver operating curve.

rate is shown on the right plot of Fig. 20 while the BDT output is shown on left plot. The latter is treated as an additional cut variable, thus cutting at a BDT output of 0.25 yields the maximal significance of ≈ 7.9 .

To further determine the BDT variables with the most impact, we drop up to two training variables and retrain the BDT without this information. The resulting BDT is evaluated on the same $\mathcal{L} = 140 \text{ fb}^{-1}$ dataset as before. The resulting drop in the significance is shown in Fig. 21.

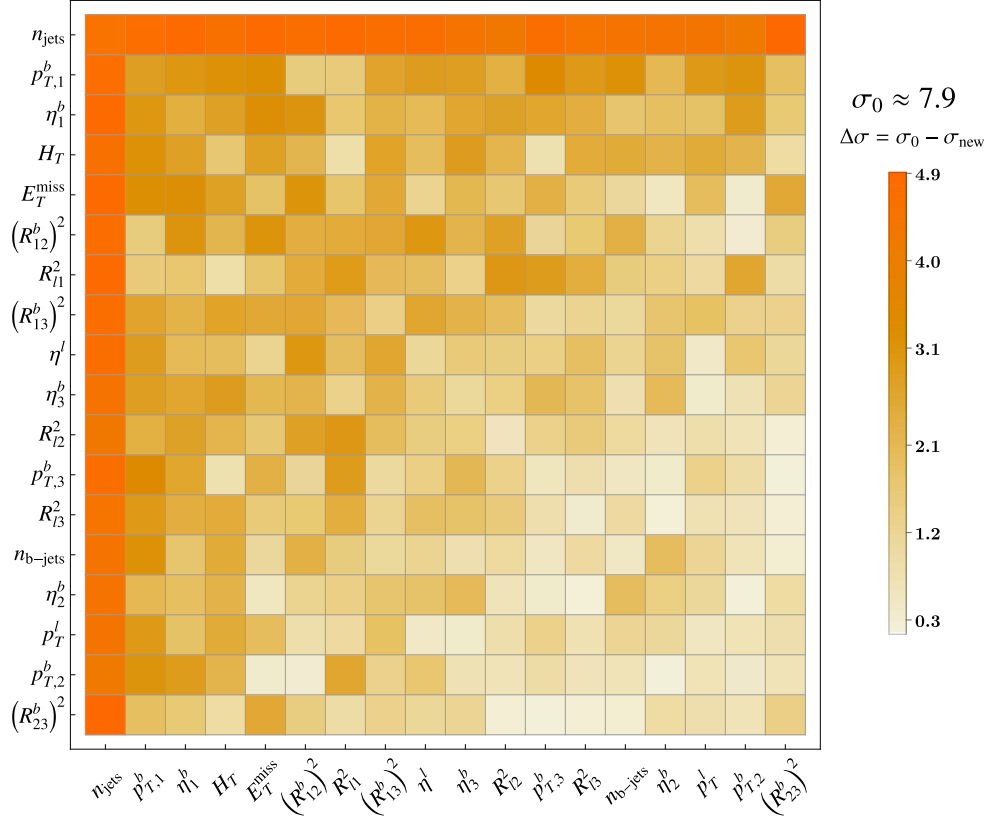


Figure 21. Change in the significance ΔZ when re-evaluating the BDT after performing the training without the variables listed on the axes. The diagonal elements correspond to dropping one training variable. The matrix is by construction symmetric. The significance using the whole set of variables is $\sigma_0 \approx 7.9$.

References

- [1] H. E. Haber and G. L. Kane, *The Search for Supersymmetry: Probing Physics Beyond the Standard Model*, *Phys. Rept.* **117** (1985) 75–263.
- [2] N. G. Deshpande and E. Ma, *Pattern of Symmetry Breaking with Two Higgs Doublets*, *Phys. Rev. D* **18** (1978) 2574.
- [3] M. Dine, W. Fischler and M. Srednicki, *A Simple Solution to the Strong CP Problem with a Harmless Axion*, *Phys. Lett.* **B104** (1981) 199–202.
- [4] A. R. Zhitnitsky, *On Possible Suppression of the Axion Hadron Interactions. (In Russian)*, *Sov. J. Nucl. Phys.* **31** (1980) 260.
- [5] V. A. Kuzmin, V. A. Rubakov and M. E. Shaposhnikov, *On the Anomalous Electroweak Baryon Number Nonconservation in the Early Universe*, *Phys. Lett. B* **155** (1985) 36.
- [6] S. L. Glashow and S. Weinberg, *Natural Conservation Laws for Neutral Currents*, *Phys. Rev. D* **15** (1977) 1958.
- [7] S. Gori, C. Grojean, A. Juste and A. Paul, *Heavy Higgs Searches: Flavour Matters*, *JHEP* **01** (2018) 108, [[1710.03752](#)].
- [8] D. Atwood, L. Reina and A. Soni, *Phenomenology of two Higgs doublet models with flavor changing neutral currents*, *Phys. Rev. D* **55** (1997) 3156–3176, [[hep-ph/9609279](#)].
- [9] A. Crivellin, A. Kokulu and C. Greub, *Flavor-phenomenology of two-Higgs-doublet models with generic Yukawa structure*, *Phys. Rev. D* **87** (2013) 094031, [[1303.5877](#)].
- [10] C.-W. Chiang, H. Fukuda, M. Takeuchi and T. T. Yanagida, *Flavor-Changing Neutral-Current Decays in Top-Specific Variant Axion Model*, *JHEP* **11** (2015) 057, [[1507.04354](#)].
- [11] M. Badziak, G. G. di Cortona, M. Tabet and R. Ziegler, *Flavor-violating Higgs decays and stellar cooling anomalies in axion models*, *JHEP* **10** (2021) 181, [[2107.09708](#)].
- [12] C.-W. Chiang, K. Fuyuto and E. Senaha, *Electroweak Baryogenesis with Lepton Flavor Violation*, *Phys. Lett. B* **762** (2016) 315–320, [[1607.07316](#)].
- [13] K. Fuyuto, W.-S. Hou and E. Senaha, *Electroweak baryogenesis driven by extra top Yukawa couplings*, *Phys. Lett. B* **776** (2018) 402–406, [[1705.05034](#)].
- [14] T. Modak and E. Senaha, *Probing Electroweak Baryogenesis induced by extra bottom Yukawa coupling via EDMs and collider signatures*, *JHEP* **11** (2020) 025, [[2005.09928](#)].
- [15] W.-S. Hou, T. Modak and T. Plehn, *A final word on FCNC-Baryogenesis from two Higgs doublets*, *SciPost Phys.* **10** (2021) 150, [[2012.03572](#)].
- [16] M. Bauer, M. Carena and K. Gemmler, *Creating the fermion mass hierarchies with multiple Higgs bosons*, *Phys. Rev. D* **94** (2016) 115030, [[1512.03458](#)].
- [17] M. Bauer, M. Carena and K. Gemmler, *Flavor from the Electroweak Scale*, *JHEP* **11** (2015) 016, [[1506.01719](#)].
- [18] W. Altmannshofer, S. Gori, A. L. Kagan, L. Silvestrini and J. Zupan, *Uncovering Mass Generation Through Higgs Flavor Violation*, *Phys. Rev. D* **93** (2016) 031301, [[1507.07927](#)].
- [19] D. Ghosh, R. S. Gupta and G. Perez, *Is the Higgs Mechanism of Fermion Mass Generation a Fact? A Yukawa-less First-Two-Generation Model*, *Phys. Lett. B* **755** (2016) 504–508, [[1508.01501](#)].

- [20] W. Altmannshofer, J. Eby, S. Gori, M. Lotito, M. Martone and D. Tucker, *Collider Signatures of Flavorful Higgs Bosons*, *Phys. Rev. D* **94** (2016) 115032, [[1610.02398](#)].
- [21] A. Dery and Y. Nir, *FN-2HDM: Two Higgs Doublet Models with Froggatt-Nielsen Symmetry*, *JHEP* **04** (2017) 003, [[1612.05219](#)].
- [22] T. D. Lee, *A Theory of Spontaneous T Violation*, *Phys. Rev. D* **8** (1973) 1226–1239.
- [23] U. Nierste, M. Tabet and R. Ziegler, *Cornering Spontaneous CP Violation with Charged-Higgs-Boson Searches*, *Phys. Rev. Lett.* **125** (2020) 031801, [[1912.11501](#)].
- [24] Y. Omura, E. Senaha and K. Tobe, *Lepton-flavor-violating Higgs decay $h \rightarrow \mu\tau$ and muon anomalous magnetic moment in a general two Higgs doublet model*, *JHEP* **05** (2015) 028, [[1502.07824](#)].
- [25] M. Arroyo-Ureña and E. Díaz, *Dipole moments of charged leptons in the THDM-III with Textures*, *J. Phys. G* **43** (2016) 045002, [[1508.05382](#)].
- [26] S.-P. Li, X.-Q. Li and Y.-D. Yang, *Muon $g - 2$ in a $U(1)$ -symmetric Two-Higgs-Doublet Model*, *Phys. Rev. D* **99** (2019) 035010, [[1808.02424](#)].
- [27] A. Celis, M. Jung, X.-Q. Li and A. Pich, *Sensitivity to charged scalars in $B \rightarrow D^{(*)}\tau\nu_\tau$ and $B \rightarrow \tau\nu_\tau$ decays*, *JHEP* **01** (2013) 054, [[1210.8443](#)].
- [28] A. Crivellin, C. Greub and A. Kokulu, *Explaining $B \rightarrow D\tau\nu$, $B \rightarrow D^*\tau\nu$ and $B \rightarrow \tau\nu$ in a 2HDM of type III*, *Phys. Rev. D* **86** (2012) 054014, [[1206.2634](#)].
- [29] C. S. Kim, Y. W. Yoon and X.-B. Yuan, *Exploring top quark FCNC within 2HDM type III in association with flavor physics*, *JHEP* **12** (2015) 038, [[1509.00491](#)].
- [30] S. Iguro and K. Tobe, *$R(D^{(*)})$ in a general two Higgs doublet model*, *Nucl. Phys. B* **925** (2017) 560–606, [[1708.06176](#)].
- [31] A. Crivellin, G. D’Ambrosio and J. Heeck, *Explaining $h \rightarrow \mu^\pm\tau^\mp$, $B \rightarrow K^*\mu^+\mu^-$ and $B \rightarrow K\mu^+\mu^-/B \rightarrow Ke^+e^-$ in a two-Higgs-doublet model with gauged $L_\mu - L_\tau$* , *Phys. Rev. Lett.* **114** (2015) 151801, [[1501.00993](#)].
- [32] S. Iguro and Y. Omura, *Status of the semileptonic B decays and muon $g-2$ in general 2HDMs with right-handed neutrinos*, *JHEP* **05** (2018) 173, [[1802.01732](#)].
- [33] S.-P. Li, X.-Q. Li, Y.-D. Yang and X. Zhang, *$R_{D^{(*)}}, R_{K^{(*)}}$ and neutrino mass in the 2HDM-III with right-handed neutrinos*, *JHEP* **09** (2018) 149, [[1807.08530](#)].
- [34] T. P. Cheng and M. Sher, *Mass Matrix Ansatz and Flavor Nonconservation in Models with Multiple Higgs Doublets*, *Phys. Rev. D* **35** (1987) 3484.
- [35] W.-S. Hou, *Tree level $t \rightarrow c h$ or $h \rightarrow t$ anti- c decays*, *Phys. Lett. B* **296** (1992) 179–184.
- [36] G. C. Branco, W. Grimus and L. Lavoura, *Relating the scalar flavor changing neutral couplings to the CKM matrix*, *Phys. Lett. B* **380** (1996) 119–126, [[hep-ph/9601383](#)].
- [37] A. Pich and P. Tuzon, *Yukawa Alignment in the Two-Higgs-Doublet Model*, *Phys. Rev. D* **80** (2009) 091702, [[0908.1554](#)].
- [38] W. Altmannshofer, S. Gori and G. D. Kribs, *A Minimal Flavor Violating 2HDM at the LHC*, *Phys. Rev. D* **86** (2012) 115009, [[1210.2465](#)].
- [39] B. Altunkaynak, W.-S. Hou, C. Kao, M. Kohda and B. McCoy, *Flavor Changing Heavy Higgs Interactions at the LHC*, *Phys. Lett. B* **751** (2015) 135–142, [[1506.00651](#)].

- [40] M. A. Arroyo-Ureña, J. L. Diaz-Cruz, E. Díaz and J. A. Orduz-Ducuaara, *Flavor violating Higgs signals in the Texturized Two-Higgs Doublet Model (THDM-Tx)*, *Chin. Phys. C* **40** (2016) 123103, [[1306.2343](#)].
- [41] F. J. Botella, G. C. Branco, M. Nebot and M. N. Rebelo, *Flavour Changing Higgs Couplings in a Class of Two Higgs Doublet Models*, *Eur. Phys. J. C* **76** (2016) 161, [[1508.05101](#)].
- [42] E. Bertuzzo, Y. F. Perez G., O. Sumensari and R. Zukanovich Funchal, *Limits on Neutrinophilic Two-Higgs-Doublet Models from Flavor Physics*, *JHEP* **01** (2016) 018, [[1510.04284](#)].
- [43] S. Gori, H. E. Haber and E. Santos, *High scale flavor alignment in two-Higgs doublet models and its phenomenology*, *JHEP* **06** (2017) 110, [[1703.05873](#)].
- [44] A. Crivellin, J. Heeck and D. Müller, *Large $h \rightarrow bs$ in generic two-Higgs-doublet models*, *Phys. Rev. D* **97** (2018) 035008, [[1710.04663](#)].
- [45] M. Kohda, T. Modak and W.-S. Hou, *Searching for new scalar bosons via triple-top signature in $cg \rightarrow tS^0 \rightarrow tt\bar{t}$* , *Phys. Lett. B* **776** (2018) 379–384, [[1710.07260](#)].
- [46] W. Altmannshofer and B. Maddock, *Flavorful Two Higgs Doublet Models with a Twist*, *Phys. Rev. D* **98** (2018) 075005, [[1805.08659](#)].
- [47] W. Altmannshofer, B. Maddock and D. Tuckler, *Rare Top Decays as Probes of Flavorful Higgs Bosons*, *Phys. Rev. D* **100** (2019) 015003, [[1904.10956](#)].
- [48] D. K. Ghosh, W.-S. Hou and T. Modak, *Sub-TeV H^+ Boson Production as Probe of Extra Top Yukawa Couplings*, *Phys. Rev. Lett.* **125** (2020) 221801, [[1912.10613](#)].
- [49] W.-S. Hou and T. Modak, *Probing Top Changing Neutral Higgs Couplings at Colliders*, *Mod. Phys. Lett. A* **36** (2021) 2130006, [[2012.05735](#)].
- [50] W.-S. Hou and T. Modak, *Prospect and implications of $cg \rightarrow bH^+ \rightarrow bAW^+$ production at the LHC*, *Phys. Rev. D* **103** (2021) 075015, [[2103.13082](#)].
- [51] M. Bordone, A. Greljo and D. Marzocca, *Exploiting dijet resonance searches for flavor physics*, *JHEP* **08** (2021) 036, [[2103.10332](#)].
- [52] S. Iguro, *Revival of H^- interpretation of $RD^{(*)}$ anomaly and closing low mass window*, *Phys. Rev. D* **105** (2022) 095011, [[2201.06565](#)].
- [53] M. Blanke, S. Iguro and H. Zhang, *Towards ruling out the charged Higgs interpretation of the $R_{D^{(*)}}$ anomaly*, [2202.10468](#).
- [54] ATLAS collaboration, G. Aad et al., *Measurement of the c -jet mistagging efficiency in $t\bar{t}$ events using pp collision data at $\sqrt{s} = 13$ TeV collected with the ATLAS detector*, *Eur. Phys. J. C* **82** (2022) 95, [[2109.10627](#)].
- [55] CMS collaboration, A. Tumasyan et al., *A new calibration method for charm jet identification validated with proton-proton collision events at $\sqrt{s} = 13$ TeV*, *JINST* **17** (2022) P03014, [[2111.03027](#)].
- [56] CMS collaboration, *Search for Higgs boson decay to a charm quark-antiquark pair in proton-proton collisions at $\sqrt{s} = 13$ TeV*, [2205.05550](#).
- [57] ATLAS collaboration, G. Aad et al., *Search for charged Higgs bosons decaying into a top quark and a bottom quark at $\sqrt{s} = 13$ TeV with the ATLAS detector*, *JHEP* **06** (2021) 145, [[2102.10076](#)].

- [58] CMS collaboration, A. M. Sirunyan et al., *Search for charged Higgs bosons decaying into a top and a bottom quark in the all-jet final state of pp collisions at $\sqrt{s} = 13$ TeV*, *JHEP* **07** (2020) 126, [[2001.07763](#)].
- [59] CMS collaboration, A. M. Sirunyan et al., *Search for a charged Higgs boson decaying to charm and bottom quarks in proton-proton collisions at $\sqrt{s} = 8$ TeV*, *JHEP* **11** (2018) 115, [[1808.06575](#)].
- [60] ATLAS collaboration, M. Aaboud et al., *Search for low-mass dijet resonances using trigger-level jets with the ATLAS detector in pp collisions at $\sqrt{s} = 13$ TeV*, *Phys. Rev. Lett.* **121** (2018) 081801, [[1804.03496](#)].
- [61] CMS collaboration, A. M. Sirunyan et al., *Search for narrow and broad dijet resonances in proton-proton collisions at $\sqrt{s} = 13$ TeV and constraints on dark matter mediators and other new particles*, *JHEP* **08** (2018) 130, [[1806.00843](#)].
- [62] ATLAS collaboration, M. Aaboud et al., *Search for low-mass resonances decaying into two jets and produced in association with a photon using pp collisions at $\sqrt{s} = 13$ TeV with the ATLAS detector*, *Phys. Lett. B* **795** (2019) 56–75, [[1901.10917](#)].
- [63] CMS collaboration, A. M. Sirunyan et al., *Search for low mass vector resonances decaying into quark-antiquark pairs in proton-proton collisions at $\sqrt{s} = 13$ TeV*, *Phys. Rev. D* **100** (2019) 112007, [[1909.04114](#)].
- [64] CMS collaboration, A. M. Sirunyan et al., *Search for dijet resonances using events with three jets in proton-proton collisions at $s=13$ TeV*, *Phys. Lett. B* **805** (2020) 135448, [[1911.03761](#)].
- [65] UFIT collaboration, M. Bona et al., *Model-independent constraints on $\Delta F = 2$ operators and the scale of new physics*, *JHEP* **03** (2008) 049, [[0707.0636](#)].
- [66] M. Bona et al. (UTfit), <http://www.utfit.org/UTfit/ResultsSummer2018>.
- [67] ATLAS collaboration, G. Aad et al., *Search for flavour-changing neutral currents in processes with one top quark and a photon using 81 fb^{-1} of pp collisions at $\sqrt{s} = 13$ TeV with the ATLAS experiment*, *Phys. Lett. B* **800** (2020) 135082, [[1908.08461](#)].
- [68] J. Alwall, M. Herquet, F. Maltoni, O. Mattelaer and T. Stelzer, *MadGraph 5 : Going Beyond*, *JHEP* **06** (2011) 128, [[1106.0522](#)].
- [69] J. Alwall, R. Frederix, S. Frixione, V. Hirschi, F. Maltoni, O. Mattelaer et al., *The automated computation of tree-level and next-to-leading order differential cross sections, and their matching to parton shower simulations*, *JHEP* **07** (2014) 079, [[1405.0301](#)].
- [70] C. Degrande, R. Frederix, V. Hirschi, M. Ubiali, M. Wiesemann and M. Zaro, *Accurate predictions for charged Higgs production: Closing the $m_{H^\pm} \sim m_t$ window*, *Phys. Lett. B* **772** (2017) 87–92, [[1607.05291](#)].
- [71] ATLAS collaboration, *Search for a light charged Higgs boson in $t \rightarrow H^\pm b$ decays, with $H^\pm \rightarrow cb$, in the lepton+jets final state in proton-proton collisions at $\sqrt{s} = 13$ TeV with the ATLAS detector*, .
- [72] C. Degrande, *Automatic evaluation of UV and R2 terms for beyond the Standard Model Lagrangians: a proof-of-principle*, *Comput. Phys. Commun.* **197** (2015) 239–262, [[1406.3030](#)].
- [73] T. Sjostrand, S. Mrenna and P. Z. Skands, *PYTHIA 6.4 Physics and Manual*, *JHEP* **05** (2006) 026, [[hep-ph/0603175](#)].

- [74] T. Sjöstrand, S. Ask, J. R. Christiansen, R. Corke, N. Desai, P. Ilten et al., *An introduction to PYTHIA 8.2*, *Comput. Phys. Commun.* **191** (2015) 159–177, [[1410.3012](#)].
- [75] S. Hoeche, F. Krauss, N. Lavesson, L. Lonnblad, M. Mangano, A. Schaliche et al., *Matching parton showers and matrix elements*, in *HERA and the LHC: A Workshop on the Implications of HERA for LHC Physics: CERN - DESY Workshop 2004/2005 (Midterm Meeting, CERN, 11-13 October 2004; Final Meeting, DESY, 17-21 January 2005)*, pp. 288–289, 2005, [hep-ph/0602031](#), [DOI](#).
- [76] M. L. Mangano, M. Moretti, F. Piccinini and M. Treccani, *Matching matrix elements and shower evolution for top-quark production in hadronic collisions*, *JHEP* **01** (2007) 013, [[hep-ph/0611129](#)].
- [77] M. Cacciari and G. P. Salam, *Dispelling the N^3 myth for the k_t jet-finder*, *Phys. Lett. B* **641** (2006) 57–61, [[hep-ph/0512210](#)].
- [78] M. Cacciari, G. P. Salam and G. Soyez, *FastJet User Manual*, *Eur. Phys. J. C* **72** (2012) 1896, [[1111.6097](#)].
- [79] M. Czakon and A. Mitov, *Top++: A Program for the Calculation of the Top-Pair Cross-Section at Hadron Colliders*, *Comput. Phys. Commun.* **185** (2014) 2930, [[1112.5675](#)].
- [80] ATLAS collaboration, *Expected performance of the ATLAS b-tagging algorithms in Run-2*, .
- [81] ATLAS collaboration, G. Aad et al., *Search for charged Higgs bosons in the $H^\pm \rightarrow tb$ decay channel in pp collisions at $\sqrt{s} = 8$ TeV using the ATLAS detector*, *JHEP* **03** (2016) 127, [[1512.03704](#)].
- [82] CMS collaboration, S. Chatrchyan et al., *Search for Resonant $t\bar{t}$ Production in Lepton+Jets Events in pp Collisions at $\sqrt{s} = 7$ TeV*, *JHEP* **12** (2012) 015, [[1209.4397](#)].
- [83] M. T. Bowen, *Using charge asymmetries to measure single top quark production at the LHC*, *Phys. Rev. D* **73** (2006) 097501, [[hep-ph/0503110](#)].
- [84] P. Ferrario and G. Rodrigo, *Massive color-octet bosons and the charge asymmetries of top quarks at hadron colliders*, *Phys. Rev. D* **78** (2008) 094018, [[0809.3354](#)].
- [85] N. Craig, C. Kilic and M. J. Strassler, *LHC Charge Asymmetry as Constraint on Models for the Tevatron Top Anomaly*, *Phys. Rev. D* **84** (2011) 035012, [[1103.2127](#)].
- [86] A. Rajaraman, Z. Surujon and T. M. P. Tait, *Asymmetric Leptons for Asymmetric Tops*, [1104.0947](#).
- [87] S. Knapen, Y. Zhao and M. J. Strassler, *Diagnosing the Top-Quark Angular Asymmetry using LHC Intrinsic charge Asymmetries*, *Phys. Rev. D* **86** (2012) 014013, [[1111.5857](#)].
- [88] P. Ko, Y. Omura and C. Yu, *Top A_{FB} at the Tevatron vs. Charge Asymmetry at the LHC in Chiral $U(1)$ Flavor Models with Flavored Higgs Doublets*, *Eur. Phys. J. C* **73** (2013) 2269, [[1205.0407](#)].
- [89] A. Kumar, J. N. Ng, A. Spray and P. T. Winslow, *Tracking down the top quark forward-backward asymmetry with monotops*, *Phys. Rev. D* **88** (2013) 075012, [[1308.3712](#)].
- [90] J. H. Kuhn and G. Rodrigo, *Charge asymmetries of top quarks at hadron colliders revisited*, *JHEP* **01** (2012) 063, [[1109.6830](#)].
- [91] M. J. Baker, J. Fuentes-Martín, G. Isidori and M. König, *High- p_T signatures in vector-leptoquark models*, *Eur. Phys. J. C* **79** (2019) 334, [[1901.10480](#)].